

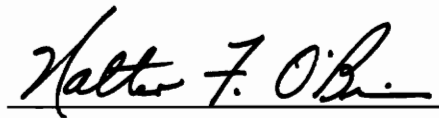
A Wide-Range Axial-Flow Compressor Stage Performance Model

by

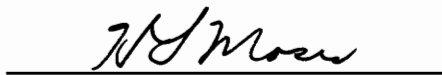
Gregory S. Bloch

Thesis submitted to the Faculty of the
Virginia Polytechnic Institute and State University
in partial fulfillment of the requirements for the degree of
MASTER OF SCIENCE
in
Mechanical Engineering

APPROVED:



W. F. O'Brien, Chairman



H. L. Moses



F. J. Pierce

July 1991

Blacksburg, Virginia

c.v

LD
5655
V855
1991
B563
C.2

A Wide-Range Axial Flow Compressor Stage Performance Model

by

Gregory S. Bloch

W. F. O'Brien, Chairman

Mechanical Engineering

(ABSTRACT)

Dynamic compression system response is a major concern in the operability of aircraft gas turbine engines. Computer models have been developed to predict compressor response to changing operating conditions. These models require a knowledge of the steady state operating characteristics as inputs, which limits the ability to use them as predicting tools.

The full range of dynamic axial flow compressor operation spans forward and reversed flow conditions. A model for predicting the wide flow range characteristics of axial flow compressor stages has been developed and a parametric study of the effect of changing design variables on steady state performance has been conducted. This model was applied to a 3-stage, low speed compressor with very favorable results and to a 10-stage, high speed compressor with mixed results.

Conclusions were made regarding the inception of stalling and the effects associated with operating a stage in a multistage environment. It was also concluded that there are operating points of an isolated compressor stage that are not attainable when that stage is operated in a multi-stage environment. A stage located in a multi-stage environment can also operate at points which cannot be reached when the stage is operated in isolation.

ACKNOWLEDGEMENTS

The author wishes to thank his advisors, Professors F. J. Pierce, H. L. Moses, and W. F. O'Brien, Chairman, for providing a unique perspective on a number of issues. The advice and guidance of Dr. O'Brien will be remembered long after completion of the degree.

The Mechanical Engineering department is recognized for providing financial assistance.

The author wishes to thank Mom Riess for her moral support. Although she "does not do graduate students," she occasionally makes exceptions for M. E. Department home boys who bring her breakfast. Special thanks go to Bob Leonard, who taught the author that all work and no play (12:02 p.m.) makes Greg a dull boy (but it is the only way to finish).

The author especially thanks his parents for all the support they have given over the years. The lessons they taught were not always learned in an expedient manner, but most of them eventually sunk in.

TABLE OF CONTENTS

LIST OF FIGURES vi

LIST OF TABLES ix

LIST OF SYMBOLS x

1 INTRODUCTION..... 1

2 LITERATURE REVIEW..... 5

3 BACKGROUND AND MODEL THEORY 11

 3.1 Forward Flow Operation..... 11

 3.1.1 Unstalled Operation..... 13

 3.1.2 Stalled Flow 18

 3.2 Reversed Flow 20

 3.3 Some Empirical Observations 23

 3.3.1 Criterion Used for Stall Inception..... 23

 3.3.2 Stalled Flow Jet Exit Angle 25

 3.3.3 Recovery Hysteresis 26

 3.3.4 Reversed Flow Pressure Calculation..... 26

 3.4 Assembly Into a Wide Range Prediction Model 27

4 APPLICATION TO A LOW SPEED COMPRESSOR 29

 4.1 Forward Flow Comparison 30

 4.2 Reversed Flow Comparison 32

5 APPLICATION TO A HIGH SPEED COMPRESSOR..... 34

 5.1 Pressure Characteristic Prediction 36

 5.2 Temperature Characteristic Prediction 39

6 PARAMETRIC INVESTIGATION OF DESIGN VARIABLES 52

6.1 The Effect of Camber on Full Range Performance..... 52

6.2 The Effect of Rotor Solidity on Full Range Performance..... 53

6.3 The Effect of Stagger on Full Range Performance 55

7 CONCLUSIONS..... 58

8 RECOMMENDATIONS..... 60

REFERENCES 62

APPENDIX A..... 65

VITA 71

LIST OF FIGURES

Figure 1. Compressor Acceleration Transient in a Turbine Engine	1
Figure 2. Compression System Surge	2
Figure 3. Compression System Stall	3
Figure 4. Equivalent Compression System Used in Greitzer Model	6
Figure 5. Full-Range Compressor Stage Characteristic	8
Figure 6. Mean Radius Section of a Compressor Stage in Forward Flow Operation	12
Figure 7. Variation of Factor m in Carter's Deviation Angle Rule [16]	14
Figure 8. Reference Minimum Loss Incidence Angle for Zero Camber [24]	15
Figure 9. Reference Minimum Loss Blade Maximum Thickness Correction [24]	15
Figure 10. Reference Minimum Loss Incidence Angle Slope Factor [24]	16
Figure 11. Correlation of Wake Momentum Thickness With Equivalent Diffusion Ratio [15]	16
Figure 12. Trailing Edge Boundary Layer Form Factor for Two-Dimensional, Low Mach Number Flow Over Compressor Airfoils [25]	17
Figure 13. Compressor Cascade Geometry and Nomenclature for Stalled Operation	19
Figure 14. Mean Radius Section of a Compressor Stage in Reversed Flow Operation	21
Figure 15. Corrected Pressure Losses in a Reversed Flow Compressor Cascade [21]	22
Figure 16. Comparison of Unstalled Axisymmetric Performance of a Research Stage in Three Different Environments [28]	24

Figure 17. Three Stage Compressor Tested by Gamache [8]	29
Figure 18. 3-Stage Test Compressor First Stage Pressure Characteristic.....	30
Figure 19. 3-Stage Test Compressor Second Stage Pressure Characteristic.....	31
Figure 20. 3-Stage Test Compressor Third Stage Pressure Characteristic	32
Figure 21. 10-Stage Test Compressor Cross Section.....	35
Figure 22. 10-Stage Compressor: a) First Stage Pressure Characteristic; b) First Stage Temperature Characteristic	42
Figure 23. 10-Stage Compressor: a) Second Stage Pressure Characteristic; b) Second Stage Temperature Characteristic	43
Figure 24. 10-Stage Compressor: a) Third Stage Pressure Characteristic; b) Third Stage Temperature Characteristic	44
Figure 25. 10-Stage Compressor: a) Fourth Stage Pressure Characteristic; b) Fourth Stage Temperature Characteristic	45
Figure 26. 10-Stage Compressor: a) Fifth Stage Pressure Characteristic; b) Fifth Stage Temperature Characteristic	46
Figure 27. 10-Stage Compressor: a) Sixth Stage Pressure Characteristic; b) Sixth Stage Temperature Characteristic	47
Figure 28. 10-Stage Compressor: a) Seventh Stage Pressure Characteristic; b) Seventh Stage Temperature Characteristic	48
Figure 29. 10-Stage Compressor: a) Eighth Stage Pressure Characteristic; b) Eighth Stage Temperature Characteristic	49
Figure 30. 10-Stage Compressor: a) Ninth Stage Pressure Characteristic; b) Ninth Stage Temperature Characteristic	50
Figure 31. 10-Stage Compressor: a) Tenth Stage Pressure Characteristic; b) Tenth Stage Temperature Characteristic	51

Figure 32. The Effect of Rotor Blade Camber on Full Range Stage Performance 53

Figure 33. The Effect of Rotor Blade Solidity on Full Range Stage Performance 54

Figure 34. Velocity Triangles Showing Effect of Increased Stagger 56

Figure 35. The Effect of Stagger on Full Range Stage Performance 57

Figure 36. A Typical Compressor Stage With Velocity Triangles for Forward
Flow Operation 66

LIST OF TABLES

Table 1. POSTALL Model Input Parameters..... 28

LIST OF SYMBOLS

A	Area
c	Blade chord
c_p	Specific heat
D_{eq}	Equivalent diffusion ratio
H	Blade span
H_2	Blade wake form factor
i	Blade incidence angle
i^*	Blade incidence angle for minimum loss operation
IGV	Inlet guide vane
M	Mach number
\dot{m}	Mass flow rate
P	Pressure
PR	Pressure ratio
R	Ideal gas constant
s	Blade spacing
T	Temperature
TR	Temperature ratio
U	Compressor wheel speed
V	Absolute velocity
W	Relative velocity

GREEK SYMBOLS

α	Absolute flow angle, or Angle of attack
β	Relative flow angle
β'	Blade metal angle
ϕ	Stage flow coefficient (defined on page 37)
δ	Flow deviation angle
γ	Blade stagger angle, or Ratio of specific heats
η	Stage efficiency
σ	Solidity
ρ	Fluid density
θ	Blade camber
θ^*	Wake momentum thickness
$\bar{\omega}$	Total pressure loss coefficient
ψ^p	Stage pressure coefficient (defined on page 37)
ψ^T	Stage temperature coefficient (defined on page 37)

SUBSCRIPTS

a	Annulus
p	Profile
R	Rotor
S	Stator
s	Secondary

x	Axial direction
0	Total property
1	Rotor or stage inlet
2	Rotor or stage exit

1 INTRODUCTION

The requirements of high performance aircraft gas turbine engines often result in operation near the compressor stall limit. For example, when a step increase in fuel flow is made, the compressor operating point initially shifts to a higher pressure ratio along a constant speed line, as shown in Figure 1. As the engine speed increases, the operating point moves to the right, following the locus of quasi-steady operating points until the new steady-state operating condition is reached.

Because maximum engine acceleration is obtained at the highest compressor pressure ratio possible, it is desirable for acceleration transients to be near the surge line. But when the compressor is operating near the stall line, a slight perturbation of the operating condition can then push the engine into stall. To allow optimization of

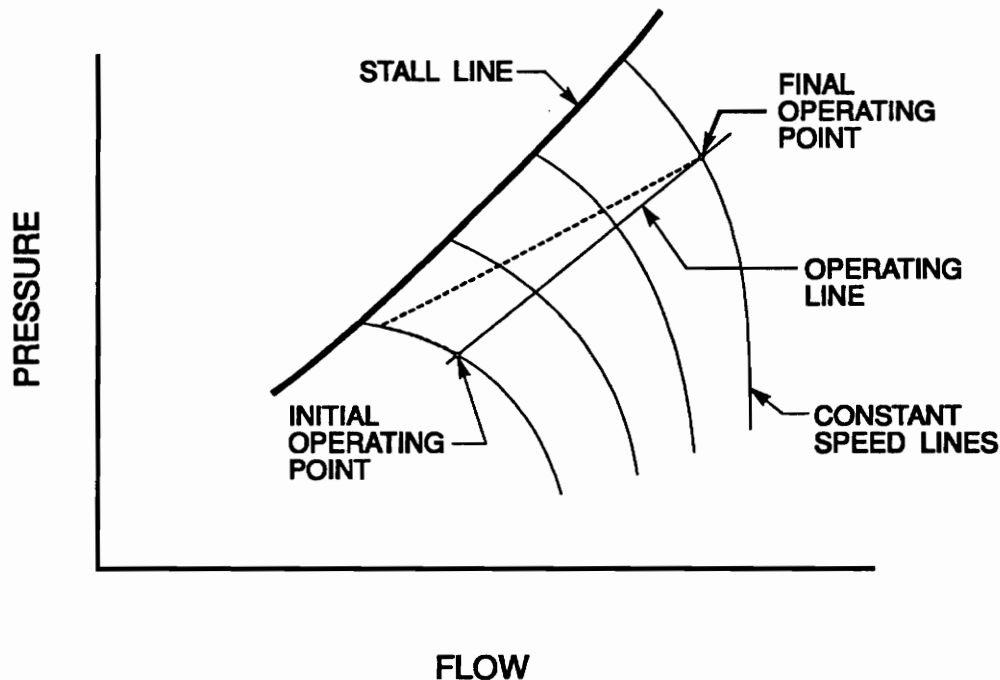


Figure 1. Compressor Acceleration Transient in a Turbine Engine

acceleration and stall margin, it is desirable to have the capability to predict transient compression system operation.

When an axial-flow compressor is operated beyond the stall limit, the two observed modes of system response are surge and rotating stall. Surge is a globally unstable phenomenon characterized by mass flow through the entire compressor oscillating between forward and reversed flow, as shown in Figure 2. During a portion of the surge cycle, the compressor operates on its unstalled performance characteristic and can, if the cause of the surge is eliminated, recover to normal operation.

Rotating stall, on the other hand, occurs when one or more blade passages become locally stalled, causing blockage of those passages only. These stall cells continually rotate around the compressor annulus, stalling the blades on the cell leading edge and unstalling the blades on the cell trailing edge. This mode of operation is undesirable because the compressor may attain globally stable operation in stall and

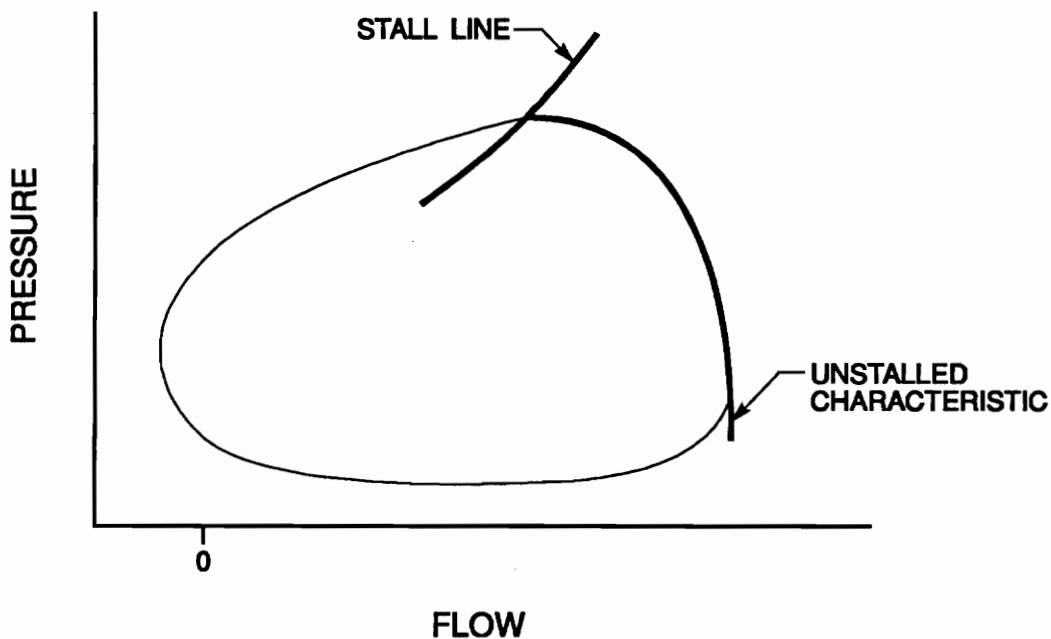


Figure 2. Compression System Surge

recovery may not be possible, even by opening the throttle to a value larger than that which initiated the stall. This results in compression system operation at reduced mass flow and pressure rise, as shown in Figure 3.

Mathematical models have been developed to predict compression system response to changes in inlet conditions, requests for acceleration and deceleration, etc. Application of these mathematical models has demonstrated that the models can be useful tools in the study of time-dependent compressor operation, including (but not limited to) stall and surge.

The successes demonstrated by these compressor modeling capabilities have established the possibility of incorporating the models into compressor design and test programs. This would give engineers the ability to evaluate the transient operation and recoverability of a compressor design before it is built, minimizing the amount of expensive wind tunnel and flight testing required. It would also allow for pre-test predictions to

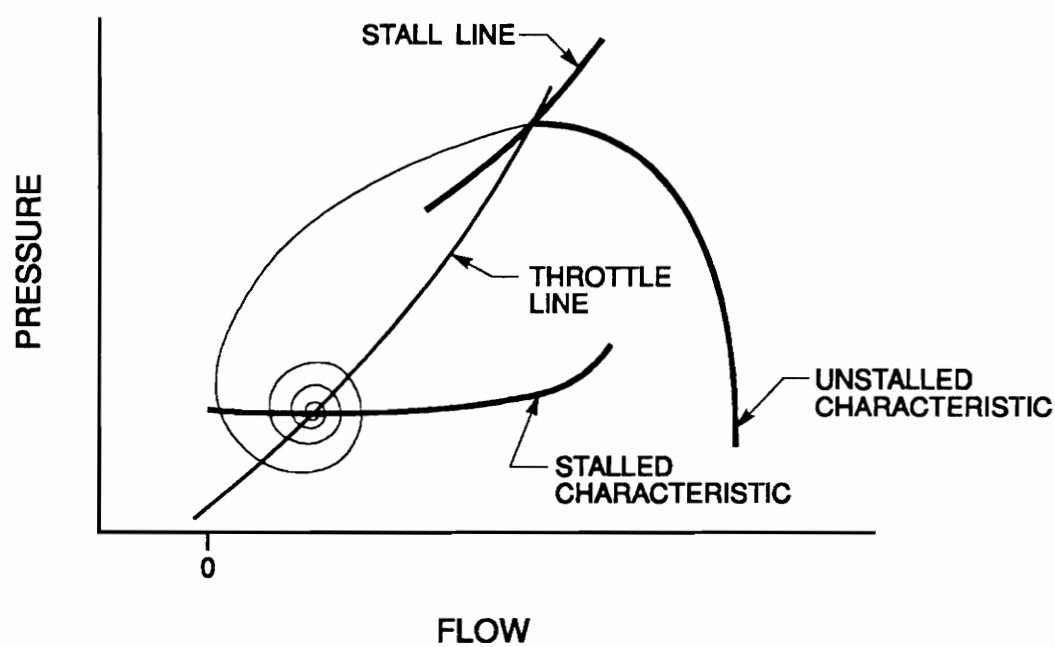


Figure 3. Compression System Stall

avoid damaging an engine during testing.

Two of the necessary inputs to dynamic performance models are the steady-state pressure and temperature characteristics for the compressor. These are currently obtained experimentally for the unstalled and, if available, rotating-stall regimes; the reversed flow characteristics can be "backed out" using surge data, but sparse surge data and the unavailability of proper instrumentation limit the usefulness of this technique.

The current reliance of dynamic compression system models on measured stage performance limits the application of these models as predictive tools. The work presented in this thesis resulted in a model for stage characteristic prediction over the entire flow regime, including the in-stall and reversed flow regions.

2 LITERATURE REVIEW

Previous investigations of wide range stage characteristics have been included as a part of dynamic compression system modeling and experiments. Because the time scale of an engine transient is of the order of several seconds and the residence time for a fluid element in an engine is of the order of 0.01 seconds, the dynamic performance is usually calculated from the steady-state characteristics.

In an effort to predict engine response to changes in throttle setting, models such as that by Saravanamuttoo and Fawke [1] were developed. These models were useful for predicting transient operation in the unstalled region, but could not predict post-stall operation or the effects of inlet distortion. Models such as that of Seldner, et. al. [2] and Kimzey [3] addressed the areas of inlet distortion and flow stability. These models showed very good agreement with the measured response, but they had actual measured data as inputs. In all cases, the authors concluded that the accurate knowledge of the steady characteristics was required to obtain this agreement.

In an effort to demonstrate qualitatively how a compressor will perform when operated beyond its normal operating region, Turner and Sparkes [4] measured the full range characteristics of a single stage axial-flow fan. This was the first report of steady reversed flow operation and it showed the general shape of the characteristics which could be expected in this flow regime, but it did not address whether the transient system response would be surge or rotating stall.

Huppert [5] showed in a qualitative way that the rotational speed and compressor exit volume affect whether a compression system will exhibit surge or stall. Experiments reported in this reference showed that for a given exit plenum, there was a speed above which the transient response was surge and below which the transient response was

rotating stall. In a similar manner, these experiments showed that for a given rotational speed, a "large" plenum would result in surge while a "small" plenum would result in stall.

In an effort to better understand the surge and stall phenomena and to quantify the effects of speed and plenum volume, Greitzer [6] developed a non-linear mathematical model to describe the transient response of an axial-flow compressor to a perturbation of the operating point. In this model, the compressor is replaced by an actuator disc pumping air through a constant area duct and into a large plenum, as shown in Figure 4. The throttle is also modeled as an actuator disc (across which the pressure drops) and a constant area duct. Although this model can capture the strongly non-linear behavior of a compression system, its application is limited to systems having a low inlet Mach number and small pressure rise compared to the ambient.

During the experimental phase of the above investigation [7], tests were conducted on a 3-stage, low-speed compressor operated at five rotational speeds while the plenum volume was varied independently. The forward-flow characteristics were measured during steady-state operation and the reversed-flow characteristics were

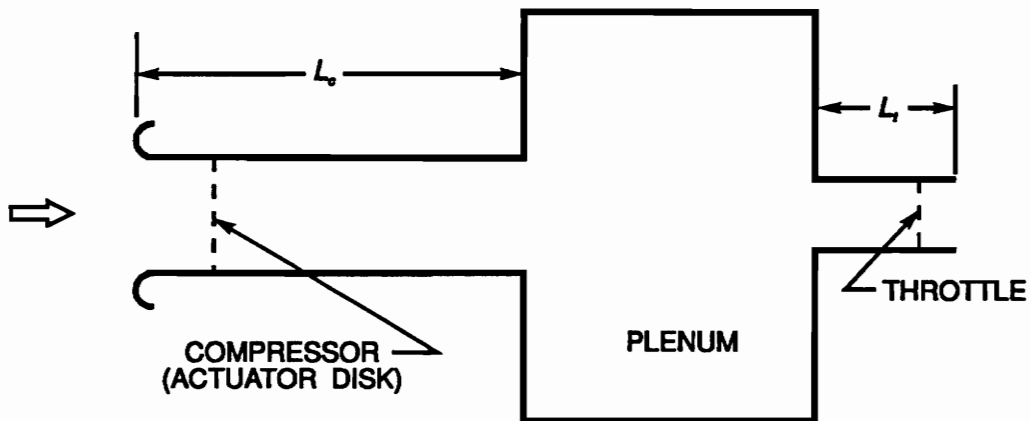


Figure 4. Equivalent Compression System Used in Greitzer Model

synthesized by inertially correcting the surge data.

The compression system response was shown to depend strongly on the value of a non-dimensional parameter, B , which relates the physical parameters of the system.

$$B = \frac{U}{2a} \sqrt{\frac{A_c}{V_p L_c}} \quad (1)$$

where a is the speed of sound, V_p is the volume of the plenum, A_c is the compressor flow-through area, and L_c is the effective length of the compressor. For a given compressor, it was shown there is a critical value of B above which the system will surge and below which it will stall. In addition, it was shown that the transient response is strongly dependent on the shape of the steady state characteristic. It was also shown that a time lag, τ , is necessary to account for the length of time required for a stall cell to develop.

Gamache [8] tested a three-stage, low-speed compressor and published the only complete characteristics for a multistage machine, including in-stall and reversed flow, in the open literature. A very steep negatively sloped characteristic was measured in the reversed flow region with a discontinuity at zero flow, as shown in Figure 5. When the measured reversed flow characteristics were used in the Greitzer model, it was shown that the discontinuity at zero flow and the steep slope in the reversed flow region strongly affected the predicted surge behavior.

Davis [9] developed a one-dimensional, stage-by-stage axial compression system mathematical model capable of predicting dynamic events in high-speed, high pressure ratio compressors. This model was applied to a three-stage, low-speed compressor and a nine stage, high-speed compressor. The individual stage and the overall pressure characteristics for the low-speed compressor were published by Gamache [8], but the stage

temperature characteristics had to be synthesized as a total temperature ratio based on the overall torque coefficient.

For the high-speed compressor, Davis estimated the unstalled pressure and temperature characteristics with the Combined Compressor Design and Evaluation Code (COCODEC) [10], but that model did not predict the point where the compressor will stall. Noting that no method existed for predicting post-stall behavior, Davis estimated the characteristics and the stall point by using the overall shape suggested by low-speed compressor tests.

Additional investigations conducted with the Davis model include examination of the in-stall and recovery behavior of a 10-stage, transonic compressor [11] and the response of a 3-stage fan to inlet temperature transients and distortion [12]. In addition to providing the first detailed validation of a state-of-the-art modeling technique, this first application provided design guidance in the area of stage loading and matching for

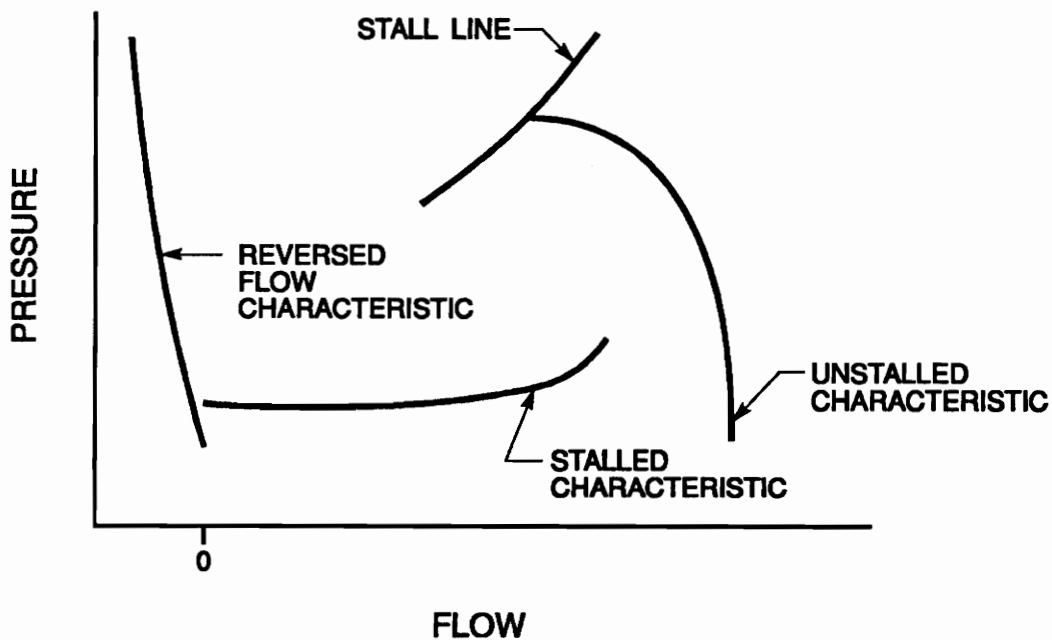


Figure 5. Full-Range Compressor Stage Characteristic

improved compressor operability.

Copenhaver [13] measured the unstalled and in-stall pressure and temperature characteristics of a 10-stage, high-speed compressor. He noted that there was a significant level of recovery hysteresis present in that compressor and that stage matching had a significant effect on in-stall performance and recovery. The time-resolved information obtained by Copenhaver was used to further validate the Davis model and again confirmed the fact that predicted compression system response is strongly dependent on the input stage characteristics.

The models reviewed thus far all required an *a priori* knowledge of the steady state stage characteristics for accurate prediction of transient response. Due to the high cost of testing an actual compressor, it is desirable to predict the compression system performance from geometry. In the case of high-speed, multi-stage compressors, the power requirements to operate the rig in reversed flow and the danger of overheating it at very low mass flows are sufficient to prevent testing in these flow regimes. All of the above information has emphasized the need to accurately predict full range stage characteristics from geometry.

The elementary two-dimensional axial-flow compressor stage analysis principles are well-known [14]. This type of analysis assumes incompressible, inviscid flow through a single stage and uses empirical correlations to estimate the pressure losses and flow deviation in each blade row. The classical correlations for these are given by Lieblein [15] and Carter [16], respectively, for unstalled operation. Once the losses have been estimated, the stage performance can be calculated.

The classical application of this blade-element theory has been limited to the prediction of near-design performance [17] because of the lack of loss and turning data for far-from-design operation. In an attempt to better understand the flow physics of

blade stalling, Yocum [18] conducted an investigation of stalled cascades and measured the angle of attack at which flow separation occurs. Ainslie [19] extended the Yocum investigation to include effects of increased solidity. The latter investigation indicated that higher solidity could delay the onset of separation only at low stagger angles. Moses and Thomason [20] have presented an approximation for the loss coefficient and fully mixed flow angle of a stalled cascade.

Carneal [21] conducted a study of cascade flow at angles representative of those encountered by a compressor operating in reversed flow. The measured losses were very large, as would be expected in this flow regime, and indicated that rotors and stators in reversed flow could be treated as equal loss producers. Suggestions for the reversed flow exit angle have been made by Turner and Sparkes [4] and by Koff and Greitzer [22].

Although there have been investigations to predict axial-flow compressor steady state characteristics in a single flow regime, the author knows of no single model which currently predicts operation over the full range. The model presented in this thesis was developed to allow pre-test stage characteristics prediction in the unstalled, stalled, and reversed flow regimes.

3 BACKGROUND AND MODEL THEORY

The model presented in this thesis, known as POSTALL4, predicts one-dimensional steady state axial flow compressor stage characteristics from two-dimensional incompressible turbomachinery principles. Conceived by O'Brien [23], the original version of the model was useful only for predicting the trends of compressor stage performance as there were no reversed flow predictions and the unstalled turning and loss models were somewhat arbitrary. The unstalled flow deviation angle was assumed to be 2° and the unstalled loss model was a curve fit in such a manner that the pressure characteristic was continuous at the transition to stall.

The work presented in this thesis involved the application of classical loss and turning models for the unstalled regime, modifying the criterion used for stall inception and the stalled flow exit angle, and the addition of a reversed flow prediction. The correlations used are taken from the published literature with a minimum of additional empiricism (discussed in Section 3.3).

3.1 Forward Flow Operation

A typical compressor stage and the flow angles associated with forward flow are shown in Figure 6. The development of the basic stage performance equations can be found in any turbomachinery textbook, so they will simply be restated here. Using the moment of momentum equation for this geometry, Euler's turbine equation gives the stage temperature rise.

$$\frac{\Delta T_0}{T_{01}} = \frac{T_{02} - T_{01}}{T_{01}} = \frac{U^2}{c_p T_{01}} \left[1 - \frac{V_{x1}}{U} \left(\frac{V_{x2}}{V_{x1}} \tan \beta_2 + \tan \alpha_1 \right) \right] \quad (2)$$

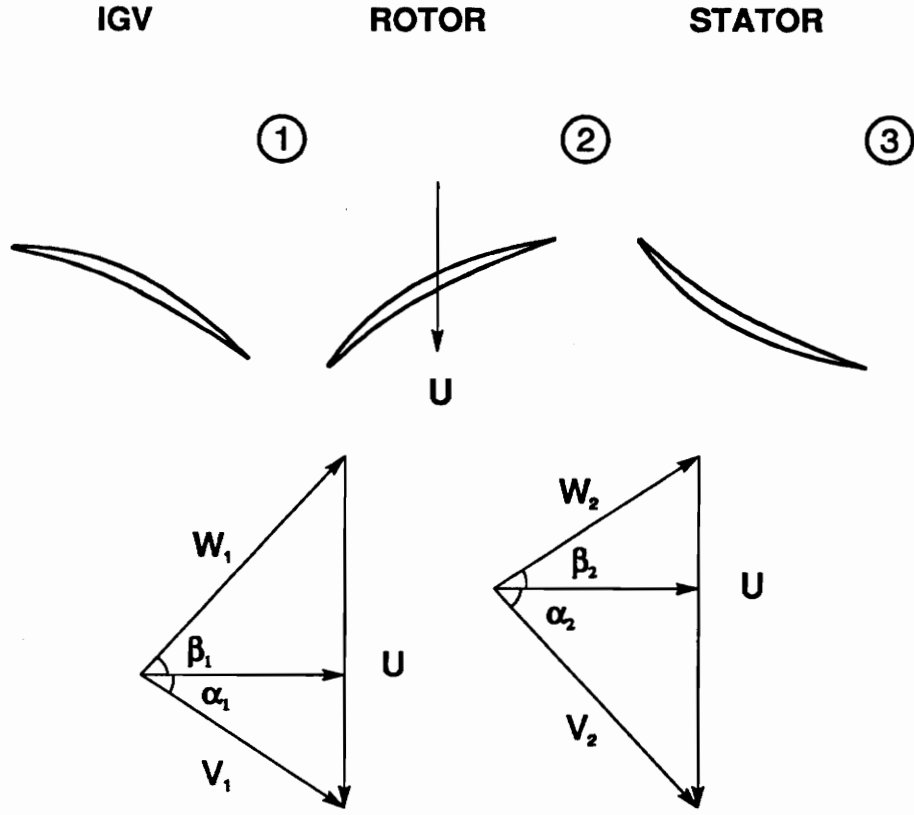


Figure 6. Mean Radius Section of a Compressor Stage in Forward Flow Operation

For incompressible flow, the total pressure rise for the stage is related to the total temperature rise and the blade row pressure losses by

$$P_{02} - P_{01} = \rho c_p \Delta T_0 - (\Delta P_{0R} + \Delta P_{0S}) \quad (3)$$

For incompressible flow, the total pressure losses are related to the cascade loss parameters by

$$\bar{\omega}_R = \frac{\Delta P_{0R}}{\rho W_1^2 / 2} \quad \text{and} \quad \bar{\omega}_S = \frac{\Delta P_{0S}}{\rho V_2^2 / 2} \quad (4)$$

For incompressible flow, the stage efficiency is given by

$$\eta = 1 - \frac{\Delta P_{0R} + \Delta P_{0S}}{\rho c_p \Delta T_0} \quad (5)$$

Since the angles in Equation (2) are flow angles and the pressure losses cannot be calculated directly, approximations for the deviation angle and loss coefficients must be made. The following two sections describe the methods used in the POSTALL4 model to estimate these in the unstalled and stalled forward flow regimes, respectively.

3.1.1 Unstalled Operation

To estimate the flow exit angle in the unstalled regime, the POSTALL4 model uses Carter's correlation [16], which is for near-design operation. Because the deviation does not change significantly until the blade stalls, this angle is assumed to be constant.

$$\beta_2 - \beta'_2 = \frac{m\theta}{\sqrt{\sigma}} \quad (6)$$

where m is obtained from Figure 7.

The blade losses are calculated as the sum of profile, annulus and secondary losses. To estimate the profile losses, the POSTALL4 model uses the correlation of Lieblein [15].

$$\bar{\omega}_p = 2\sigma \frac{\cos^2 \beta_1}{\cos^3 \beta_2} \left(\frac{\theta^*}{c} \right)_2 \left\{ \frac{\frac{2H_2}{3H_2 - 1}}{\left[1 - \left(\frac{\theta^*}{c} \right)_2 \frac{\sigma H_2}{\cos \beta_2} \right]^3} \right\} \quad (7)$$

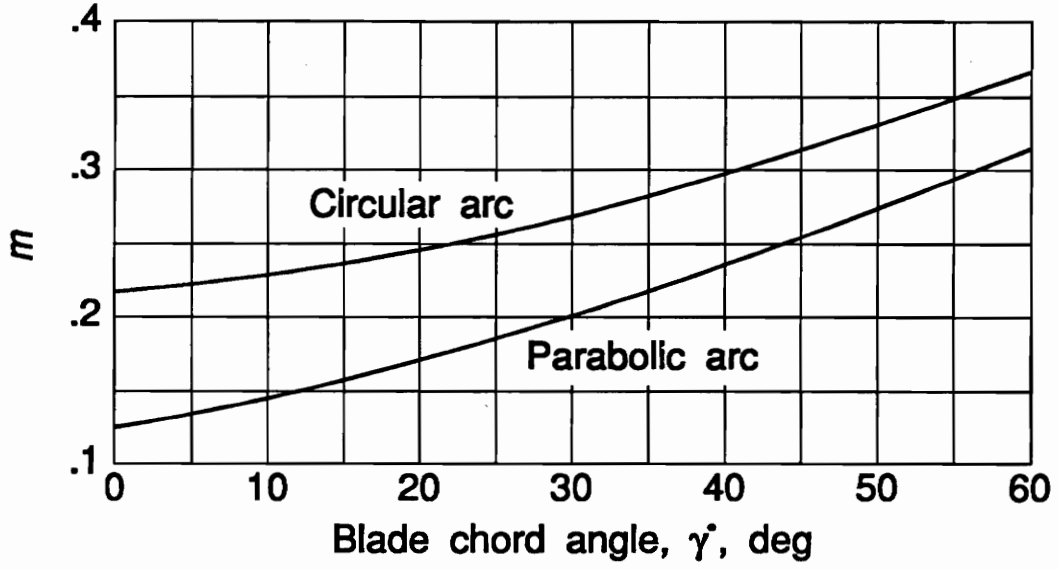


Figure 7. Variation of Factor m in Carter's Deviation Angle Rule [16]

The calculation of the terms in the above equation begins with the determination of the minimum loss incidence for the blade row, as given by Lieblein [24].

$$i^* = K_{sh} K_t i_0 + n\theta \quad (8)$$

In this relation, i_0 is the minimum loss incidence for an uncambered 10 percent thick blade, as shown in Figure 8; K_{sh} is a correction for blade shape and is taken as 0.7 for circular arc blades and 1.0 for NACA 65-series blades; K_t is a correction for maximum thickness, as shown in Figure 9; n is the slope of the incidence angle variation with camber, as shown in Figure 10.

With the minimum loss incidence thus calculated, the equivalent diffusion ratio is given by Lieblein [15].

$$D_{eq} = \frac{\cos \beta_2}{\cos \beta_1} \left[1.12 + a(i - i^*)^{1.43} + 0.61 \frac{\cos^2 \beta_1}{\sigma} (\tan \beta_1 - \tan \beta_2) \right] \quad (9)$$

where $a = 0.0117$ for NACA 65-series blades and $a = 0.007$ for circular arc blades.

Once the equivalent diffusion ratio is calculated, the trailing edge momentum thickness can be read from Figure 11.

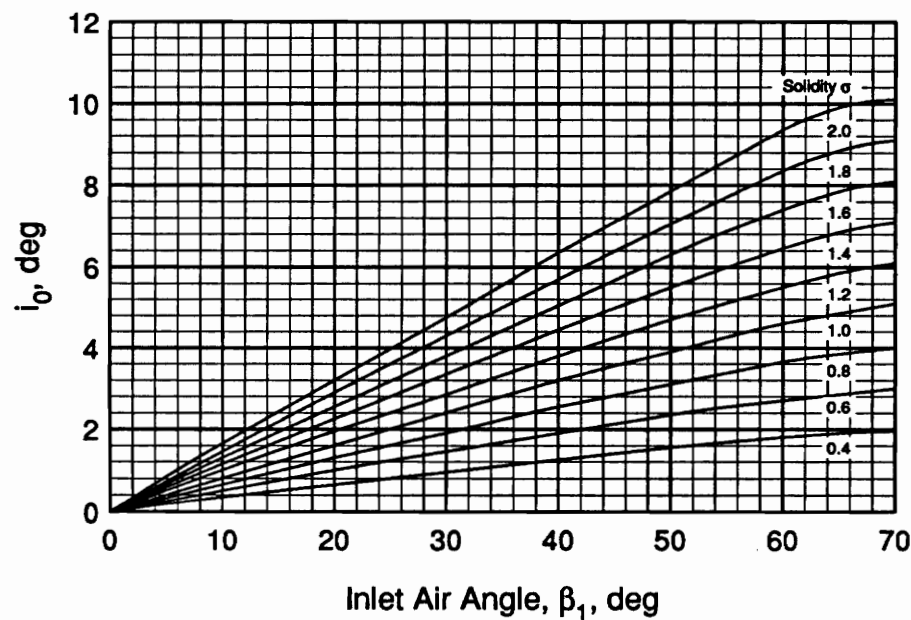


Figure 8. Reference Minimum Loss Incidence Angle for Zero Camber [24]

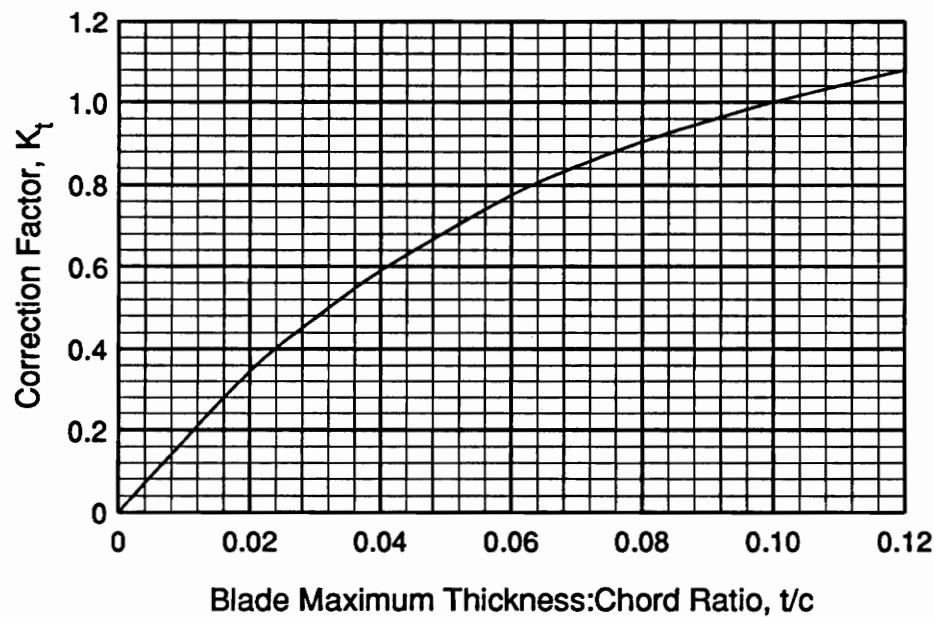


Figure 9. Reference Minimum Loss Blade Maximum Thickness Correction [24]

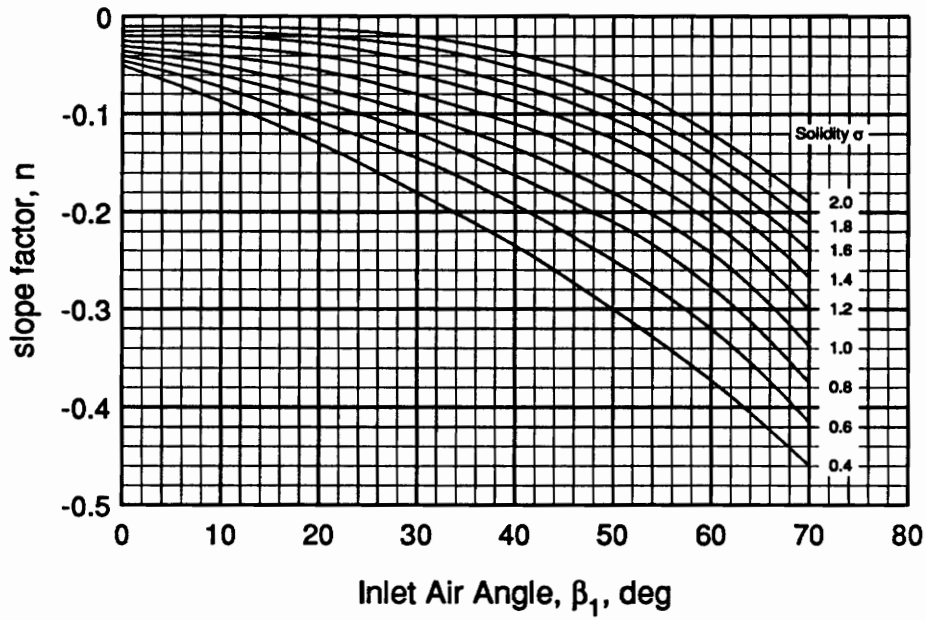


Figure 10. Reference Minimum Loss Incidence Angle Slope Factor [24]

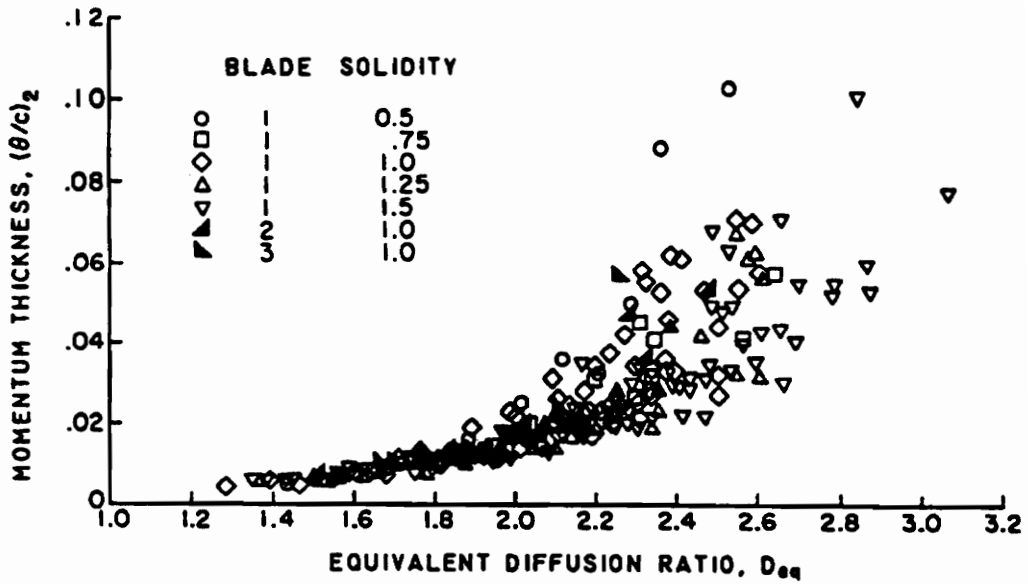


Figure 11. Correlation of Wake Momentum Thickness With Equivalent Diffusion Ratio [15]

For the trailing edge form factor, Lieblein [15] suggested a constant $H_2 = 1.08$ be used, but the POSTALL4 model uses the Koch and Smith [25] correlation shown in Figure 12, which is based on more modern data.

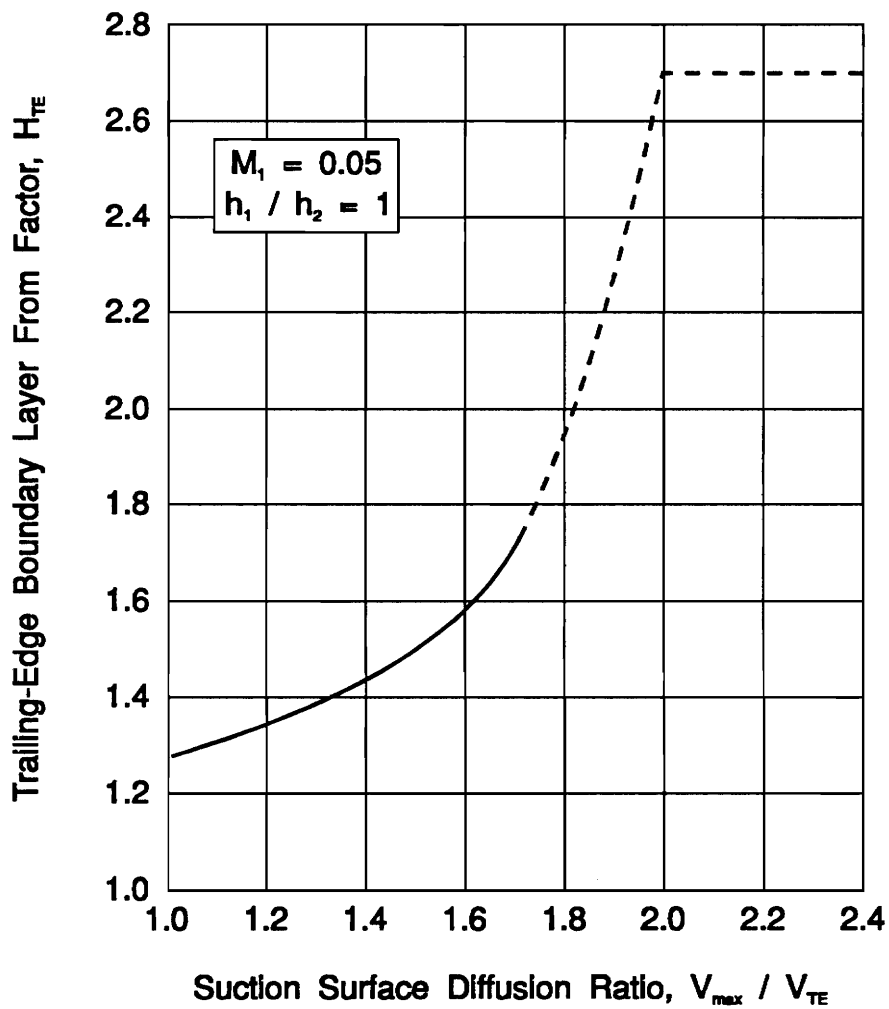


Figure 12. Trailing Edge Boundary Layer Form Factor for Two-Dimensional, Low Mach Number Flow Over Compressor Airfoils [25]

To complete the calculation of the unstalled blade row losses, Dixon [26] provides the following estimates of the annulus and secondary losses.

$$\bar{\omega}_a = 0.02 \sigma \left(\frac{c}{H} \right) \frac{\cos^2 \beta_1}{\cos^3 \beta_m} \quad \text{where } \tan \beta_m = \frac{(\tan \beta_1 + \tan \beta_2)}{2} \quad (10)$$

$$\bar{\omega}_s = \frac{0.072}{\sigma} \frac{\cos^2 \beta_1}{\cos \beta_m} (\tan \beta_1 - \tan \beta_2)^2 \quad (11)$$

3.1.2 Stalled Flow

For stalled operation, the flow is assumed to separate from the blade leading edge, as shown in Figure 13, and the approximation of Moses and Thomason [20] is used to predict the fully mixed flow angle and loss coefficient. The determination of the jet exit angle, β_2 , is based on some additional empiricism and is discussed in Section 3.3.2. The jet velocity ratio is given by

$$\frac{V_2}{V_1} = \frac{-b \pm \sqrt{b^2 - 4ac}}{2a} \quad (12)$$

where

$$a = 1 + \frac{0.15\sigma}{\cos \beta_1}$$

$$b = \frac{-2 \cos \beta_1 \cos \delta}{\cos \gamma} \quad c = \frac{2 \cos \beta_1 \cos \alpha}{\cos \gamma} - 1$$

To give meaningful results, only the positive result in Equation 12 is used.

The fully mixed flow angle and loss coefficient are given by

$$\tan \beta_3 = \frac{V_2 \sin \beta_2}{V_1 \cos \beta_1} \quad (13)$$

$$\bar{\omega} = \frac{p_{01} - p_{03}}{\rho V_1^2 / 2} = \left(1 + \frac{0.15\sigma}{\cos \beta_1}\right) \frac{V_2^2}{V_1^2} + 2 \cos \beta_1 \left(\cos \beta_1 - \frac{V_2}{V_1} \cos \beta_2 \right) - \frac{\cos^2 \beta_1}{\cos^2 \beta_3} \quad (14)$$

Because the profile losses for a stalled blade row are much larger than the annulus and secondary losses, the latter are ignored in this flow regime.

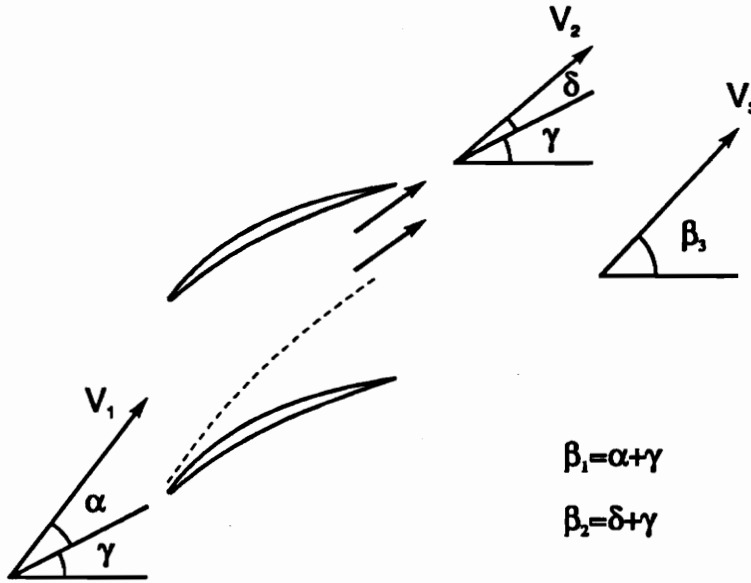


Figure 13. Compressor Cascade Geometry and Nomenclature for Stalled Operation

3.2 Reversed Flow

A typical compressor stage and the flow angles associated with reversed flow are shown in Figure 14. The development of the basic stage performance equations are a direct extension of those presented in Section 3.1 with the subscripts changed to reflect the direction of flow. Using the moment of momentum equation for this geometry, Euler's turbine equation gives the stage temperature rise.

$$\frac{\Delta T_0}{T_{02}} = \frac{T_{02} - T_{01}}{T_{02}} = \frac{-U^2}{c_p T_{02}} \left[1 - \frac{V_{x1}}{U} \left(\frac{V_{x2}}{V_{x1}} \tan \alpha_2 + \tan \beta_1 \right) \right] \quad (15)$$

It should be noted that the compressor does work on the fluid in the direction of flow, increasing its temperature in that direction. When the compressor is operating in reversed flow, the temperature at station 1 is greater than at station 2 and the result in Equation (15) is negative. The flow angle, β_1 , is assumed to be the blade metal angle as suggested by Turner and Sparkes [4] and by Koff and Greitzer [22]. The mixing calculations described in Section 3.1.2 are not performed because the discriminant in Equation (12) is often negative.

For incompressible flow in the reversed direction, the pressure rise for the stage is related to the temperature rise and the blade row losses as follows. It is noted that the pressure losses are *added* in this equation because they are positive in the direction of flow, which is from station 2 to station 1.

$$P_{02} - P_{01} = \rho c_p \Delta T_0 + (\Delta P_{0R} + \Delta P_{0S}) \quad (16)$$

Carneal [21] showed that cascade losses in the reversed flow region, when non-dimensionalized by wheel speed, collapse onto a single parabola as shown in Figure 15.

Although the loss curve for one stagger angle diverges from the others at reversed flow coefficients less than -0.25 , the region of compressor operation is $V_x/U \geq -0.25$, even during a deep surge cycle. The implication of this result is that the reversed flow losses are reasonably approximated as a function of mass flow only, independent of flow angle, solidity, blade shape, and other flow details. The POSTALL4 code uses a parabola fit to the five coincident curves of Carneal's data to determine the blade row losses as a function of mass flow and this result is used in Equation (16) to calculate the stage pressure rise.

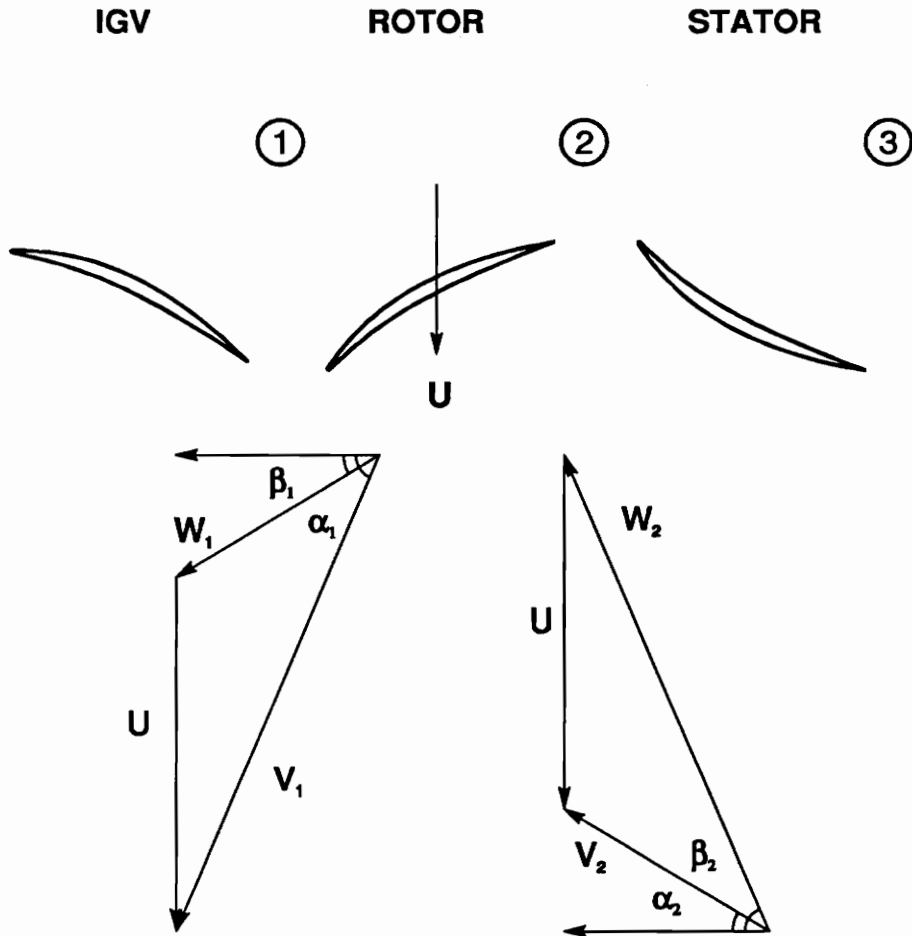


Figure 14. Mean Radius Section of a Compressor Stage in Reversed Flow Operation

Gamache [8] noted that the last stage stator in reversed flow functions in the same manner as the IGV during forward flow. The flow enters the blade row with a small angle of attack and is turned from the axial direction, accelerating the flow like a nozzle. Gamache measured a negligible pressure loss across this blade row in reversed flow operation, so the POSTALL4 code neglects the losses for the last stator of the compressor when operating in reversed flow.

The stage efficiency is not a meaningful number in reversed flow because the large pressure losses in the reversed flow analog of Equation (5) (page 13) and the use of correction factors discussed in Section 3.3.4 often make the result fall outside of the bounds of $0 \leq \eta \leq 1$.

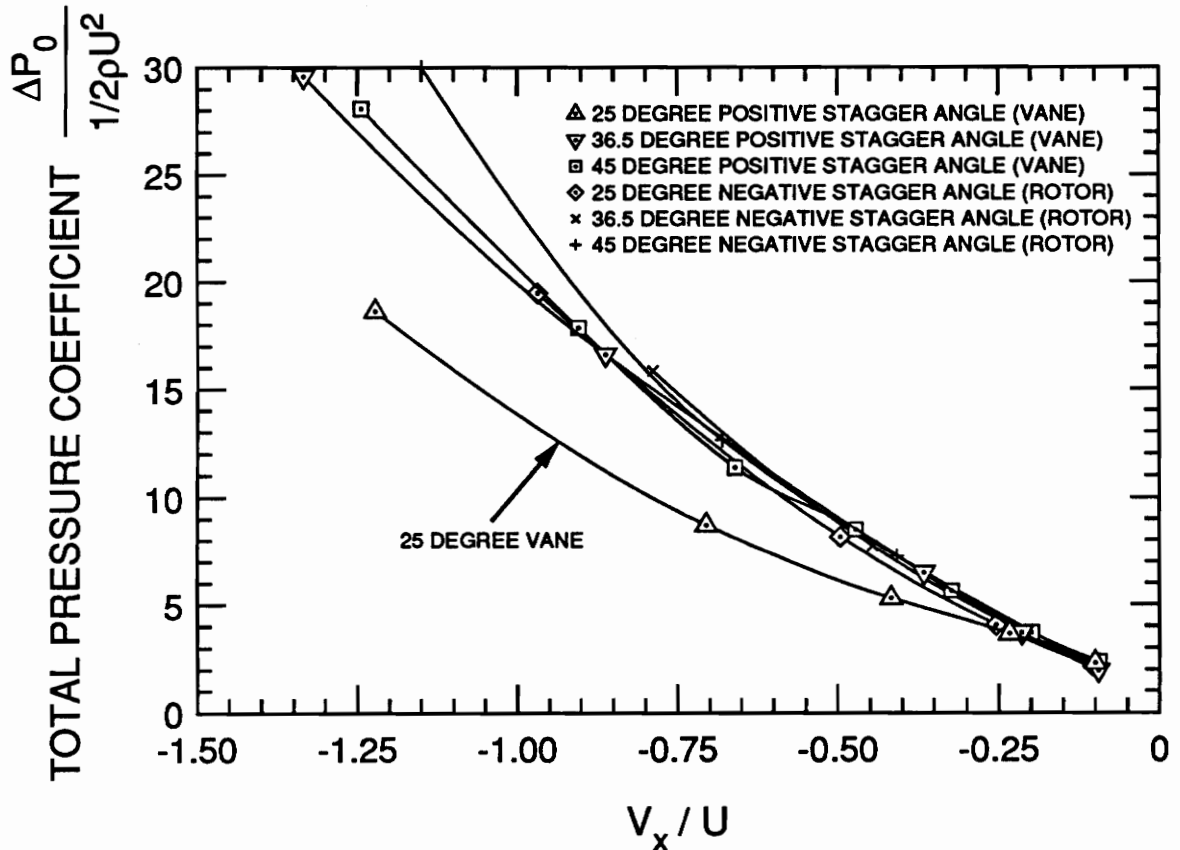


Figure 15. Corrected Pressure Losses in a Reversed Flow Compressor Cascade [21]

3.3 Some Empirical Observations

Although the POSTALL4 model is based on first principles, some empirical information is required. The published correlations used in the model have been described in the preceding sections, but some additional empiricism has been necessary to achieve the desired agreement with measured characteristics. These additions were based on a logical extension of the published literature, whenever possible, and are presented below.

3.3.1 Criterion Used for Stall Inception

Yocum [18] reported the angle of attack at which flow separation would occur in a test cascade to be 17° . Initial application of this stalling criterion [27] yielded excellent prediction of the stall point of the 3-stage, low speed compressor tested by Gamache [8], but predicted stalling would occur at much higher flow rates than were actually measured on the 10-stage, high speed rig tested by Copenhaver [13]. Further investigation indicated that use of the angle of attack as the stalling criterion would limit the application of the model to machines with similar camber, and that the angle of incidence would be a better criterion.

The blades tested by Yocum had a circular arc camber line and 18° of camber, so separation occurred at 8° incidence. Application of this stalling criterion produced very good agreement with the stall point for the last stage of the Gamache compressor and the last two stages of the Copenhaver compressor, but agreement was progressively worse towards the front of both machines.

Longley and Hynes [28] reported that a stage operating as part of a multistage compressor can remain unstalled at flows much lower than the isolated clean flow stall point, as shown in Figure 16. It has been suggested by Cousins [29] that the pumping action of the downstream stages tends to prevent upstream flow separation. In an attempt

to model this effect, the angle of incidence at which separation occurs is assumed to be the sum of the isolated stall incidence (8°) and a correction for the location of the stage in a multistage environment. This leads to the following expression for stalling incidence.

$$i_{stall} = 8^\circ + a\Delta i \quad (17)$$

where
$$a = \frac{\text{current stage\#} - 1}{\text{total \# stages} - 1} \quad \Delta i = i_{measured\ stall} - 8^\circ$$

The measured stall incidence was the actual incidence at which the first stage of the Gamache compressor stalled (16°). The bounds this puts on the incidence angle for separation are $8^\circ \leq i_{stall} \leq 16^\circ$, with 8° used for the last stage and 16° used for the first stage. This correlation was applied to all stages modeled and reported in this thesis.

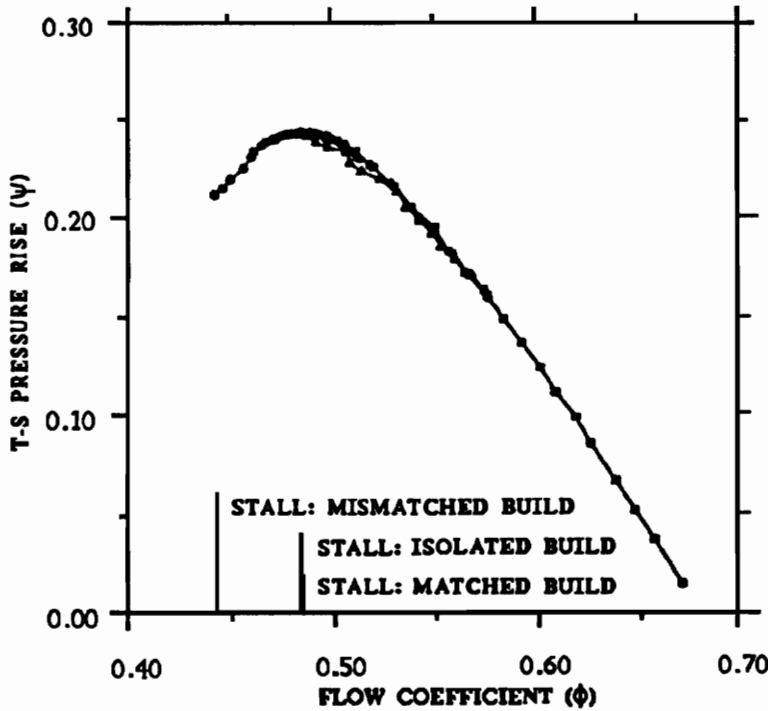


Figure 16. Comparison of Unstalled Axisymmetric Performance of a Research Stage in Three Different Environments [28]

When a blade row stalls, the flow at the trailing edge consists of a high velocity jet near the pressure surface and a separated, recirculating region near the suction surface. It is expected that the wake will not have sufficient time to mix to a uniform condition before reaching the downstream blade row and that the recirculating region will be sufficient to initiate stall of the downstream row. For this reason, the POSTALL4 model assumes that when the rotor stalls, the downstream stator stalls as well.

3.3.2 Stalled Flow Jet Exit Angle

The reasoning used to determine the stalled flow jet exit angle is similar to that presented in the previous section. The approximation of Moses and Thomason [20] suggests that the flow leaves the trailing edge at approximately the stagger angle. This was found to predict the stalled flow well for the last stage of the Gamache [8] compressor and the last three stages of the Copenhagen [13] compressor, but under-predicted the stalled pressure rise for the first two Gamache stages and the middle stages of the Copenhagen rig. It is suggested that the same mechanism which delays the onset of stall in the upstream stages tends to reduce the extent of separation once stall occurs.

The jet angle is assumed to be the sum of the trailing edge blade angle and a correction for the location of the stage in a multistage environment. This gives the following correlation for the jet exit angle.

$$\beta_2 = \beta'_2 + a(\beta'_2 - \gamma) \quad (18)$$

where
$$a = \frac{\text{current stage\#} - 1}{\text{total \# stages} - 1}$$

The bounds this puts on the jet exit angle are $\beta'_2 \leq \beta_2 \leq \gamma$, with the lower bound of β'_2 being used for the first stage and γ for the last stage. This correlation was applied to all stages modeled and reported in this thesis.

3.3.3 Recovery Hysteresis

It is well-known [30] that a compressor will not recover from stall until the mass flow is increased to a value greater than that which existed when stall was initiated, but the extent of the hysteresis that will be present is not well understood. The POSTALL4 model predicts the stage performance in this region where the characteristics are double valued, but does not attempt to address the extent of the hysteresis. In addition to performing the unstalled calculations, the stalled flow calculations are attempted beginning with the incidence 6° before stall inception. This amount of hysteresis is somewhat arbitrary and was decided upon because it is the amount of hysteresis present in the first stage of the Gamache compressor. Because the stalled calculations involve solving the quadratic in Equation (12), solution is not possible for all incidence angles and not all of the predicted stage characteristics presented show the full 6° of hysteresis.

3.3.4 Reversed Flow Pressure Calculation

The flow field in a compressor operating in reversed flow is not well understood, as there has been little research performed in this flow regime. The experiments published by Gamache [8] are the only reversed flow characteristics for a multistage compressor in the open literature. The POSTALL4 model predicts reversed flow performance as described in Section 3.2, but an empirical correction has been added to Equation (16) to improve agreement. The pressure rise in annulus reversed flow is calculated as

$$P_{02} - P_{01} = a_1 \rho c_p \Delta T_0 + a_2 (\Delta P_{0R} + \Delta P_{0S}) + a_3 \quad (19)$$

$$\text{where } a_1 = 0.31$$

$$a_2 = 1.33$$

$$a_3 = 0.20$$

with the blade row loss calculated as discussed in Section 3.2.

These coefficients were developed by matching the pressure prediction for the first stage of the Gamache compressor with the measured characteristic (*before* the last two stages were modeled); the same coefficients were then applied to all stages modeled and reported in this thesis. It should be noted that at this time there is no theory to explain these coefficients; they are strictly empirical.

3.4 Assembly Into a Wide Range Prediction Model

To obtain the range of mass flow coefficients in the forward flow regime, the relative flow angle at the rotor inlet is varied from zero angle of attack to zero flow (relative flow angle is 90°) in one degree increments. The flow is initially unstalled and the method outlined in Section 3.1.1 is used to predict the unstalled stage characteristics. When the rotor incidence exceeds the value at which stalling occurs, the method outlined in Section 3.1.2 is used to calculate in-stall performance. To generate the reversed flow characteristics, the POSTALL4 model increments the mass flow index, V_x/U , by a fixed (negative) amount and the method outlined in Sections 3.2 and 3.3.4 is used to calculate annulus reversed flow performance.

The information required by the POSTALL4 model to predict stage performance is the rotor and stator mean-radius geometry, as summarized in Table 1.

Table 1. POSTALL Model Input Parameters

rotor blade leading edge angle
rotor blade trailing edge angle
rotor blade stagger angle
rotor blade mean radius
number of rotor blades
rotor blade chord
rotor blade span
rotor blade thickness/chord ratio
IGV or (upstream) stator exit flow angle
stator blade leading edge angle
stator blade trailing edge angle
stator blade stagger angle
stator blade mean radius
number of stator blades
stator blade chord
stator blade span
stator blade thickness/chord ratio
stage axial velocity ratio
location (stage number) of stage being modeled
number of stages in the machine being modeled

4 APPLICATION TO A LOW SPEED COMPRESSOR

To verify the accuracy of the POSTALL4 technique, the code was used to predict the performance of the low-speed 3-stage rig tested by Gamache and shown in Figure 17. This compressor had a constant flowpath annulus with 3 non-repeating stages; further details about this compressor can be found in Reference 8. For this machine, a stage was defined as a rotor and the downstream stator.

The predicted and measured pressure characteristics for this machine are presented in Figures 18 through 20 (pages 30 through 32). The predicted characteristics showed very good qualitative agreement in the forward flow region and excellent agreement in the reversed flow region. The POSTALL4 prediction has the same curvature as the measured characteristic throughout the entire flow regime and has no

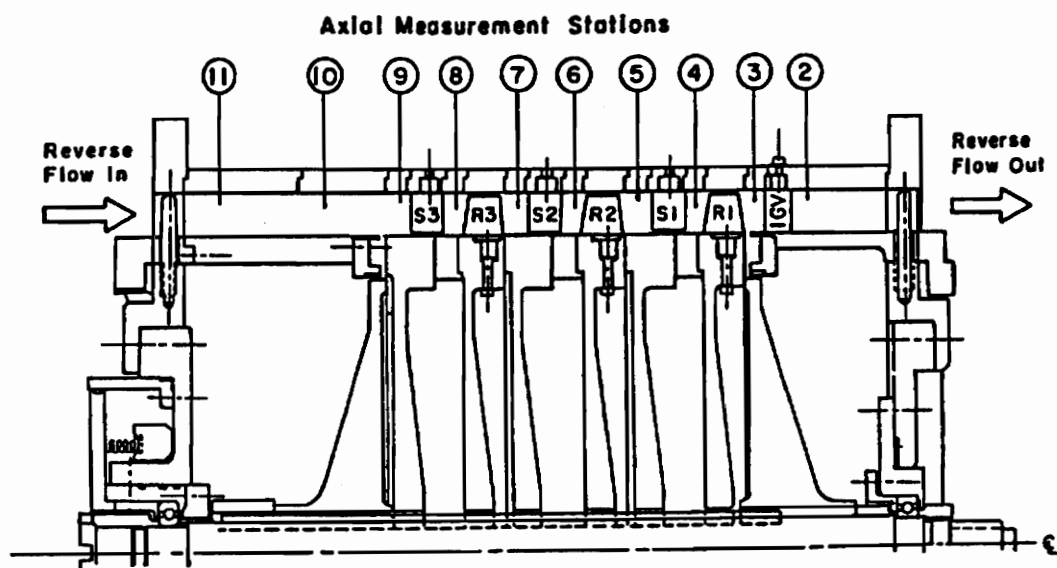


Figure 17. Three Stage Compressor Tested by Gamache [8]

unexplained discontinuities. Although it is not indicated in Figures 18 and 19, the measured characteristics for stages 1 and 2 exhibited a good deal of scatter near zero flow, but were too closely spaced to distinguish individual data points. The data shown are representative.

4.1 Forward Flow Comparison

For all 3 stages of this machine, the POSTALL4 model predicted the flow coefficient, V_x/U , for transition to abrupt stall within 0.01 of the measured value. It should be noted that this difference between predicted and measured transition represents an error of less than 1° angle of incidence to the rotor.

3-Stage Test Compressor

First Stage Pressure Characteristic

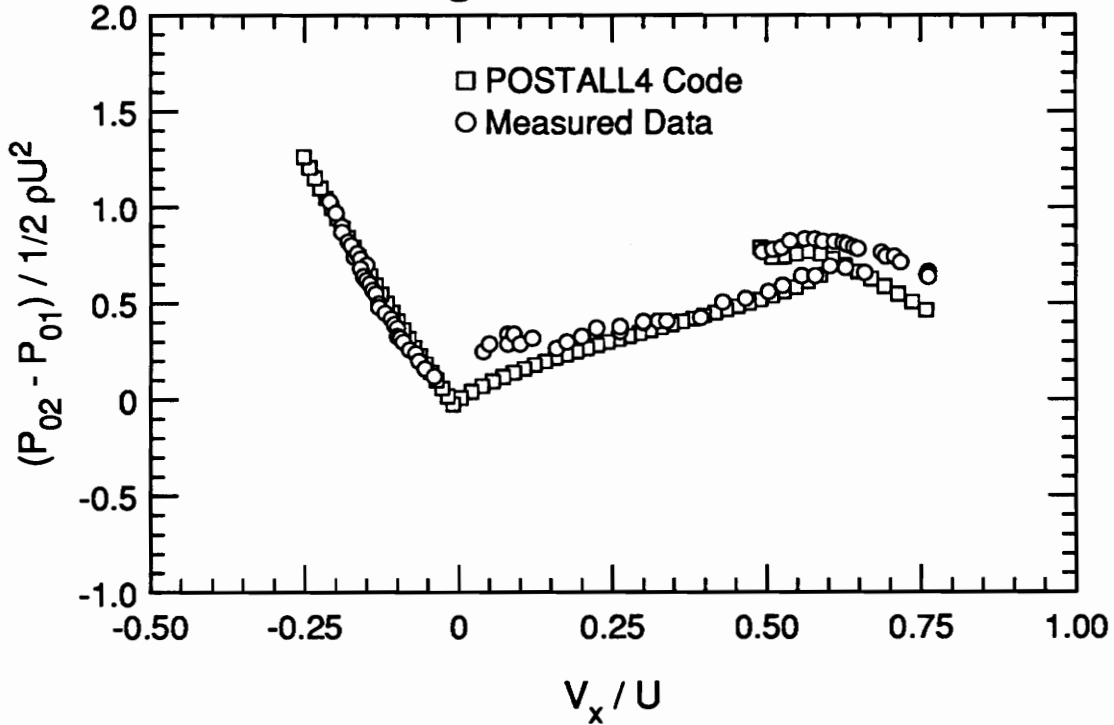


Figure 18. 3-Stage Test Compressor First Stage Pressure Characteristic

The unstalled pressure prediction was within 0.15 of the measured values for the first and third stages, but the second stage agreement was not as good. This is attributed, at least in part, to a potential lack of correct geometry to describe the compressor. The table in Reference [8] that contains the stage geometry is inconsistent, as the difference between the leading and trailing edge blade angles does not equal the value published for camber for all stages. The unstalled prediction for the second stage was within 0.20 of the measured values.

3-Stage Test Compressor

Second Stage Pressure Characteristic

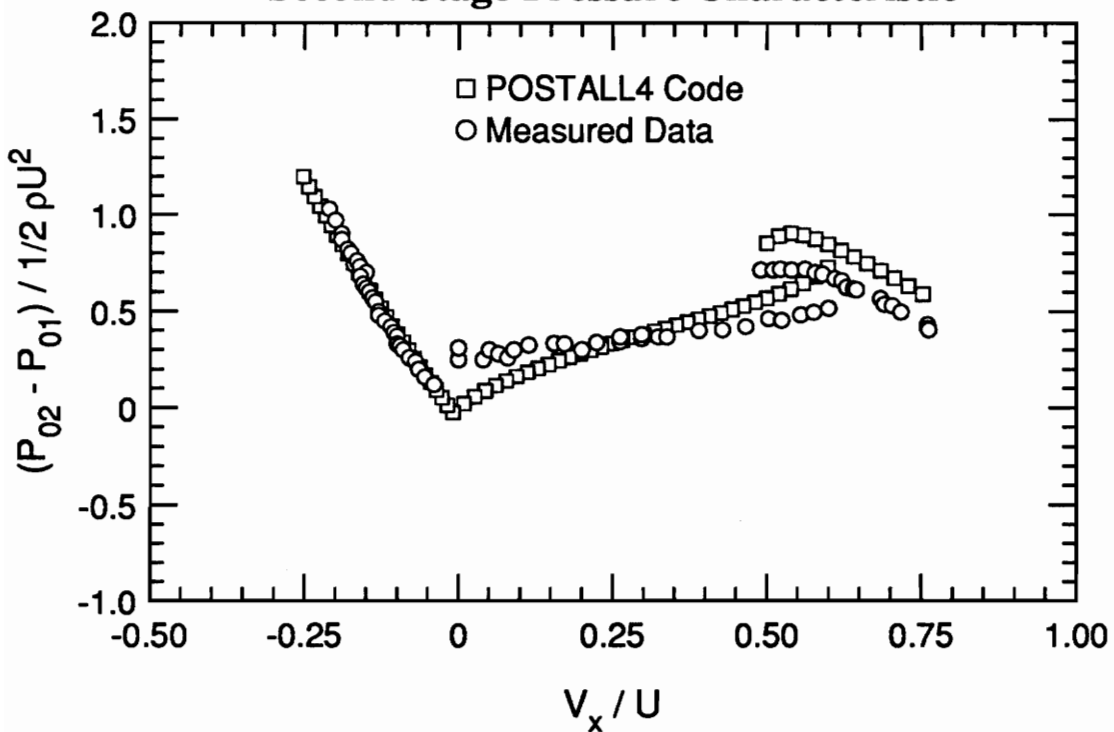


Figure 19. 3-Stage Test Compressor Second Stage Pressure Characteristic

3-Stage Test Compressor

Third Stage Pressure Characteristic

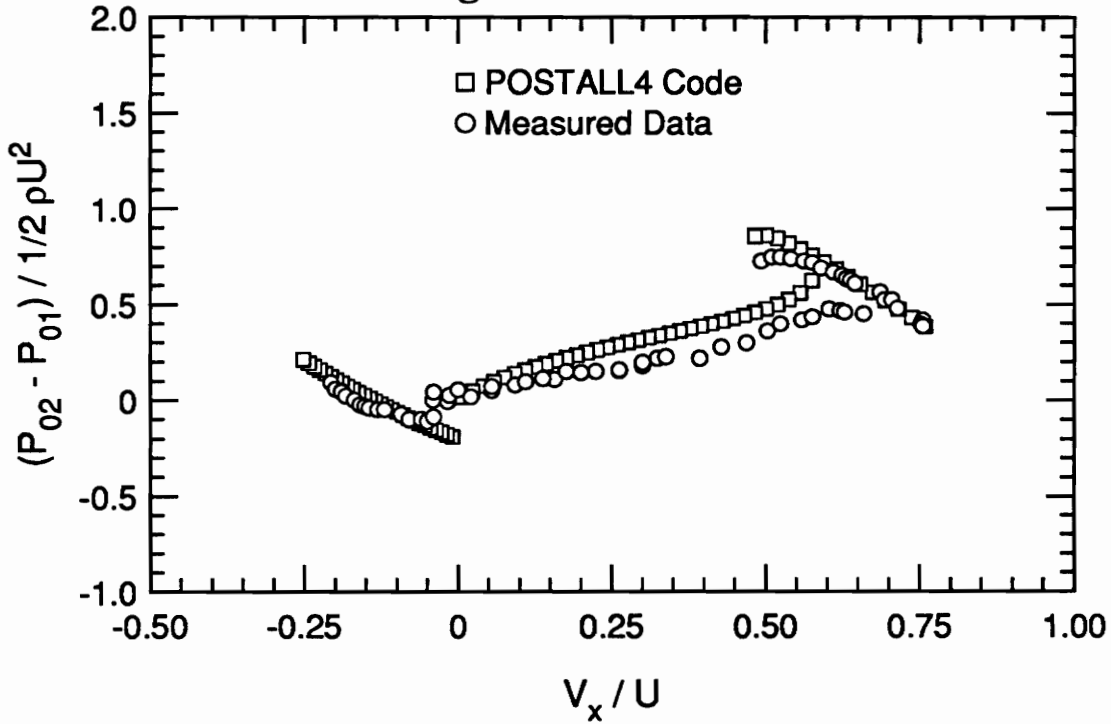


Figure 20. 3-Stage Test Compressor Third Stage Pressure Characteristic

For flow coefficients greater than 0.10, approximately 90% of the in-stall data were within 0.10 of the predicted pressure characteristic. The general shape of the POSTALL4 characteristic is the same for all stages, reaching a zero pressure rise at zero flow, while many compressors exhibit some positive pressure rise at zero flow. The mechanisms for this observed phenomenon are not currently understood.

4.2 Reversed Flow Comparison

The first stage reversed flow pressure prediction is coincident with the measured characteristic, as would be expected (this was the one stage used to develop the correction factors described in Section 3.3.4). Application of these correction factors to

the second stage prediction yielded an essentially exact match to the characteristic. This is in good qualitative agreement with the results of Carneal [21] that indicated that both rotors and stators in reversed flow could be treated as nearly equal loss producers. For both of these stages, the slope of the characteristic is very steep. This is because the blade row losses in reversed flow are very large, as shown in Figure 15, and a large pressure is required at station 2 to force air through the stage.

The reversed flow pressure prediction for the third stage is within 0.07 of the corresponding measured values. The more nearly horizontal characteristic for this stage is the result of the last stator in reversed flow operating in the same manner as the IGV in forward flow. Because there are small pressure losses in the last stator row (as compared to the first two stator rows), a smaller pressure at the stage exit will force flow backwards through this stage.

5 APPLICATION TO A HIGH SPEED COMPRESSOR

The POSTALL4 code was used to model the performance of the 10-stage high-speed compressor tested by Copenhaver [13] and shown in Figure 21. This compressor was the high pressure compressor from a modern high-performance aircraft gas turbine engine and was tested at five speeds ranging from 49.8% to 78.5% of design corrected speed to investigate stalling and recovery behavior. The modeled and measured stage pressure and temperature characteristics are presented in Figures 22 through 31 (pages 42 through 51). The flow, pressure, and temperature coefficients plotted in these figures are defined as follows.

$$\phi = \frac{\left[\frac{\dot{m}\sqrt{T_0}}{P_0 A} \right] [\text{NC}]}{0.5318} \quad (20)$$

$$\psi^T = [\text{TR} - 1][\text{NC}]^2 \quad (21)$$

$$\psi^P = \left[\text{PR}^{\frac{\gamma-1}{\gamma}} - 1 \right] [\text{NC}]^2 \quad (22)$$

$$\text{where } [\text{NC}] = \frac{\left[\left(\frac{N}{\sqrt{\theta}} \right)_{\text{design}} \right]}{\left[\left(\frac{N}{\sqrt{\theta}} \right)_{\text{actual}} \right]} \quad \text{and} \quad \theta = \frac{T_0}{T_{\text{ref}}}$$

Because the POSTALL4 model assumes incompressible flow across a single stage, the predicted stage characteristics are independent of wheel speed and the

measured data are presented without distinction of the speed at which they were obtained.

When reviewing the part speed operation of a multistage compressor, it is instructive to look at the effect of density variation on stage performance. Under low speed conditions, the density increase across the each stage is lower than the design value. The area reduction found in high speed, multi-stage compressors results in high axial velocities in the rear stages and can lead to choking. The choke-limited mass flow then results in high angles of attack and stalling in the front stages. This is the classical starting problem discussed by Graham and Guentert [30].

To aid in engine starting, virtually all modern multi-stage axial compressors use mass flow bleeds in the middle stages and/or variable-stagger inlet guide vanes and stators. By closing the variable IGVs and stators, the stage characteristics are shifted to the left on the mass flow axis, as will be demonstrated in the next section, while the use of bleeds shifts the operating line for the stages upstream of the bleeds to the right on the characteristic. The use of one or both of the above allows the front stages to operate on the unstalled portion of their characteristics, providing the needed density increase which

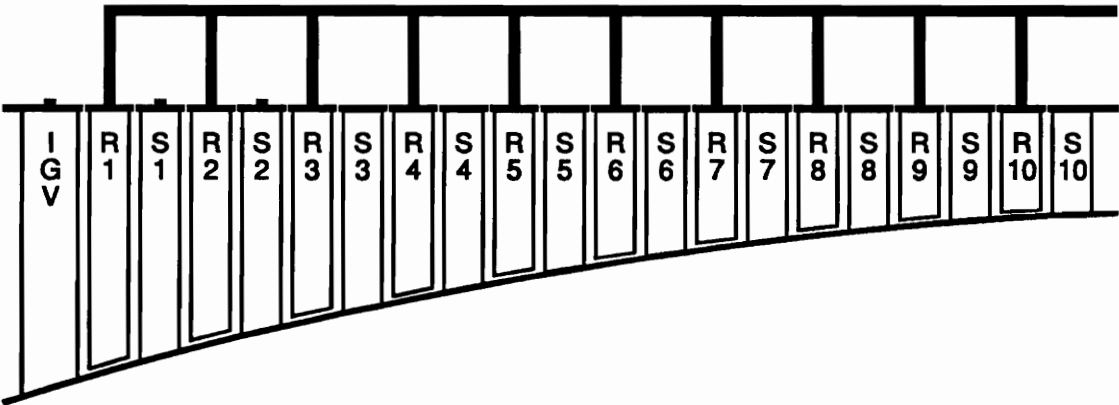


Figure 21. 10-Stage Test Compressor Cross Section

will reduce the axial velocity in the rear stages and allow them to operate nearer their design point.

Before discussing the pressure and temperature characteristics, a comment regarding the flow coefficient predictions are in order. The POSTALL4 code predicted the transition to stall within 2° angle of incidence to the rotor for all stages in the compressor. At this point it is unknown whether this is the result of an underlying mechanism that is approximated but not yet understood (as discussed in Section 3.3.1) or whether this is a fortuitous coincidence.

5.1 Pressure Characteristic Prediction

The POSTALL4 code consistently over-predicted the pressure coefficients for the first three stages by a significant amount for reasons that are not clearly understood, but for which two theories are put forth. Both involve compressibility effects which the POSTALL4 code is currently unable to model.

In the first stages of a high speed multi-stage compressor, there is a significant amount of area reduction to account for the on-design density increase as the flow progresses through the machine. This area reduction is intended to account for a phenomenon that the incompressible POSTALL4 model is incapable of capturing.

For the low corrected speeds at which this compressor was tested, the IGV and first two stator rows were fully closed (large stagger angles, as measured from an axial reference). Under these conditions, the flow into the IGV is at a large angle of incidence and is turned a significant amount away from the axial direction. The large incidence is likely to cause separation from the IGV leading edge, causing large pressure losses. This situation is far from normal IGV operation and the current model is unable to approximate these losses accurately. A second effect of the closed vanes is that the flow is accelerated significantly due to the reduction in apparent flow area. This area ratio is

of sufficient magnitude to cause choking of the flow (even at moderately low mass flow), a phenomenon which the POSTALL4 model is incapable of predicting.

Based on the nearly vertical pressure characteristic for the second stage and the vertical characteristic for the third stage, Copenhaver [13] concluded that choking existed in these stages. Because these stages appeared choked at high flow coefficients, and because of the negatively sloped pressure characteristics for the entire operating region, Copenhaver concluded that they were operating in a high-flow manner under all conditions. Based on the flow angles calculated by the POSTALL4 model, this author suggests that the stages were operating in-stall when the mass flow was low enough to eliminate the choking. The fact that there is good agreement between the predicted in-stall pressure rise and the measured performance for the second and third stages would tend to support this suggestion.

The pressure prediction for the fourth stage presents mixed results. The prediction in the high flow region is in fairly good agreement with the measured performance, but the lower flow unstalled prediction diverges from the measured values in a manner similar to the predictions of the first three stages. The in-stall prediction for this stage has the same slope as the measured performance, but is significantly lower in magnitude. It is interesting to note that the rather arbitrary amount of hysteresis modeled (discussed in Section 3.3.3) appears to duplicate the actual hysteresis present.

The unstalled pressure predictions for the fifth, sixth, and seventh stages showed excellent agreement with the measured performance. The POSTALL4 characteristics are literally coincident with the actual data points. The in-stall predictions have the same slope as the measured characteristics, but are significantly lower in magnitude. As with the fourth stage, the amount of hysteresis assumed appears to be the same as what is actually present.

The pressure prediction for the eighth stage shows good agreement with the measured performance in both the unstalled and in-stall regions, but the transition to stalled operation was not predicted very well. A miscalculation of 2° angle of incidence to the rotor is present. The unstalled prediction is slightly higher than the actual characteristic, but the difference in the stalled prediction is smaller than that of the upstream stages.

The unstalled pressure prediction for the ninth stage showed good qualitative agreement with the measured data, but the two characteristics diverge as the flow coefficient is increased. This is likely the result of the high velocity flow which exists at the back of a high speed multi-stage compressor operating at part speed. The stalled prediction agrees very well with the measured data for flow coefficients less than approximately 0.45, but at higher mass flows the POSTALL4 model significantly over-predicts the pressure rise. It is worth noting that the rather arbitrary amount of hysteresis assumed is *not* correct for this stage.

The unstalled pressure prediction for the tenth stage agrees well with the measured data for flow coefficients less than 0.60. At higher mass flows, the high velocity air at the stage entrance causes the pressure to *drop* and the stage performs like a turbine. When operated in-stall, the tenth stage was extracting work from the flow for all data points, with an obvious choking condition at a flow coefficient of 0.57. For these reasons, the predicted and measured performance were not even close.

Before discussing the reversed flow pressure characteristics, it should be noted that the instrumentation placed on this compressor resulted in a stage being defined as a stator followed by a downstream rotor. There are two implications of this stage definition in reversed flow. The first implication is that there is no "last stage stator" for which the losses should be neglected, because the tenth stator is not part of a stage for which

performance was measured; the tenth stage consists of stator 9 and rotor 10. The second implication is that the effect of the fully closed IGV and first two stators in reversed flow will only be seen in the first and second stages; stator 3 will control the flow angle into stage 2, stator 2 will control the flow angle into stage 1 and flow downstream of the IGV in reversed flow is outside of the compressor.

The predicted reversed flow pressure characteristics are essentially identical for all but the first and second stages. The coincident characteristics for the last eight of the ten stages is in good qualitative agreement with the characteristics measured by Gamache [8] for the first two stages of that compressor. The reason the POSTALL4 model predicted the smaller (magnitude) slope for the first two stages is because the IGV and first two stators are closed to the flow path. This resulted in a larger relative flow angle into the first and second rotors and more work being done on the air in the reversed direction. Because of the experimental difficulty of generating reversed flow in high-speed, high-pressure ratio compressors, no reversed flow data were obtained.

5.2 Temperature Characteristic Prediction

The unstalled temperature predictions for the first three stages are higher than the measured characteristics, but show good qualitative agreement. The predicted temperature rise is approximately correct at stall inception, but at lower mass flow the measured temperature rise increases much more than the POSTALL4 model predicts. This is believed to be the result of the significant viscous heating which occurs at low flow rates in high speed compressors.

At this time, an interesting point can be made about the perceived inception of stall. In the unstalled region, both the POSTALL4 code and the measured temperature rise show a linear characteristic with negative slope. It is clear from the first, fourth, and fifth stage data that the temperature characteristic experiences a discontinuous change in

slope and curvature at the inception of stall (as defined by the slope of the pressure characteristic) and this is confirmed by the POSTALL4 model. Since the change in slope of the temperature characteristic is much more pronounced than that of the pressure curve, it is suggested that temperature performance may be a better indicator of stall inception. In reference to the performance of the second and third stages, the temperature characteristics would indicate that at flow coefficients less than 0.30 and 0.33, respectively, these stages are operating in-stall.

The unstalled temperature prediction for the fourth and fifth stages showed excellent agreement with the measured performance. The characteristics were almost coincident in this region. The in-stall predictions for these stages show the same trend of under-predicted temperature rise at low mass flow that was shown by the first three stages, but this trend is much less pronounced for the fourth stage.

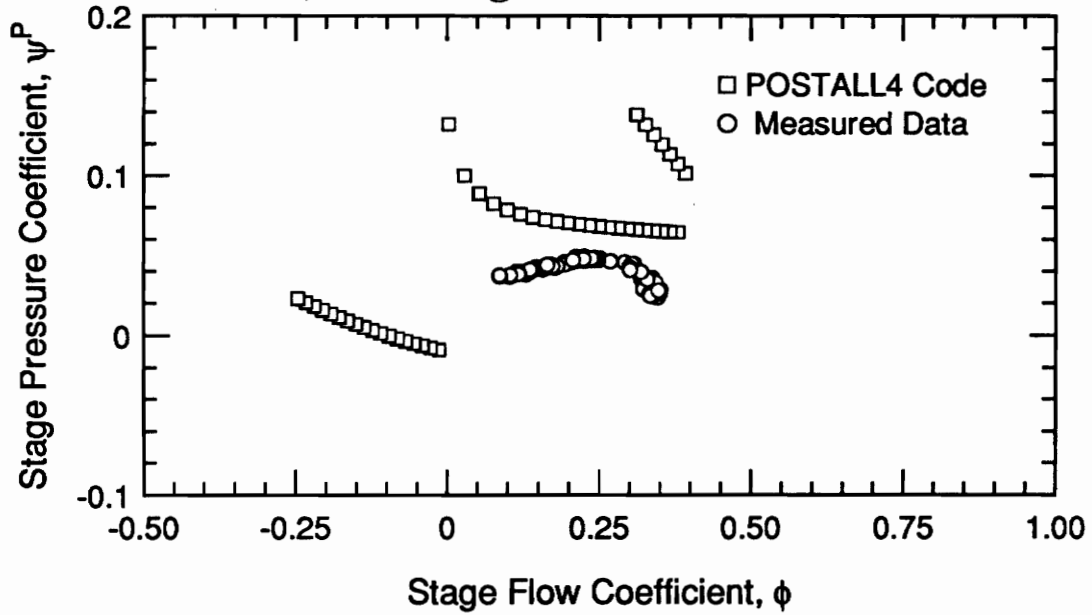
For all stages, the reversed flow temperature prediction is positively sloped and linear. The slope of the temperature characteristic is larger for the first two stages than for the last eight. This is because the IGV and first two stators are fully closed to the flow path, creating a larger relative flow angle to the rotor and resulting in higher turning. There are currently no reversed flow data for this compressor, so comparisons cannot be made.

The predicted temperature rise for unstalled operation of the sixth through tenth stages shows excellent agreement with the measured performance. A large fraction of the predictions are literally coincident with the data. The in-stall temperature predictions for these stages are of the same form as for the first five stages, but the measured characteristics are positively sloped and linear. The measured data show a steady state *drop* in temperature with an increase in pressure, which violates the second law of thermodynamics, for a portion of the stalled characteristic. Copenhaver [13] suggested

that the indicated drop in temperature was the result of significant recirculating flow within the rotating stall cells. As the flow moved backwards through each stage, work was done on it and its temperature increased. For the sixth through ninth stages, the slope of the measured in-stall characteristic is the same as the slope of the predicted reversed flow characteristic, which would tend to support this theory. All of the above predictions must be viewed as the result of an axisymmetric model. The model cannot presently account for two- and three-dimensional, non-uniform effects which may influence the flow field.

10-Stage Test Compressor

a) First Stage Pressure Characteristic



b) First Stage Temperature Characteristic

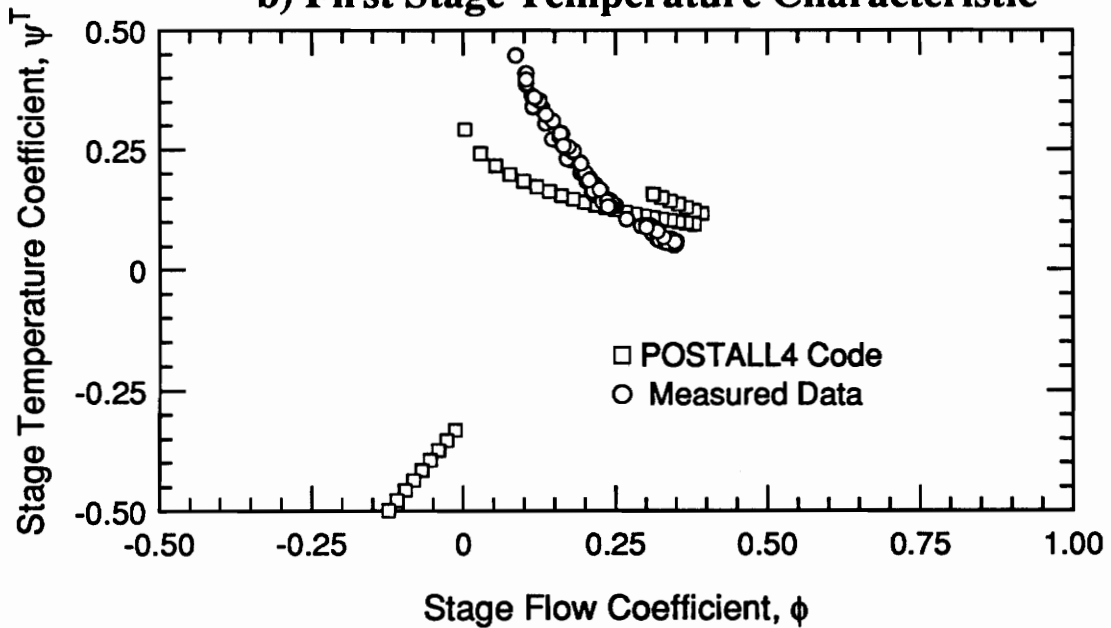
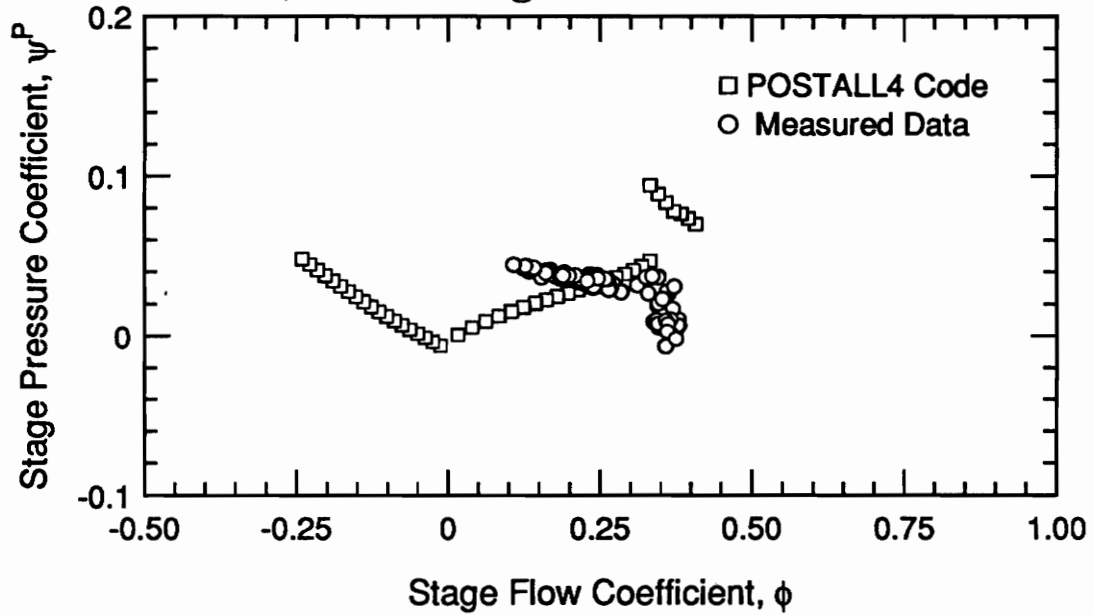


Figure 22. 10-Stage Compressor: a) First Stage Pressure Characteristic; b) First Stage Temperature Characteristic

10-Stage Test Compressor

a) Second Stage Pressure Characteristic



b) Second Stage Temperature Characteristic

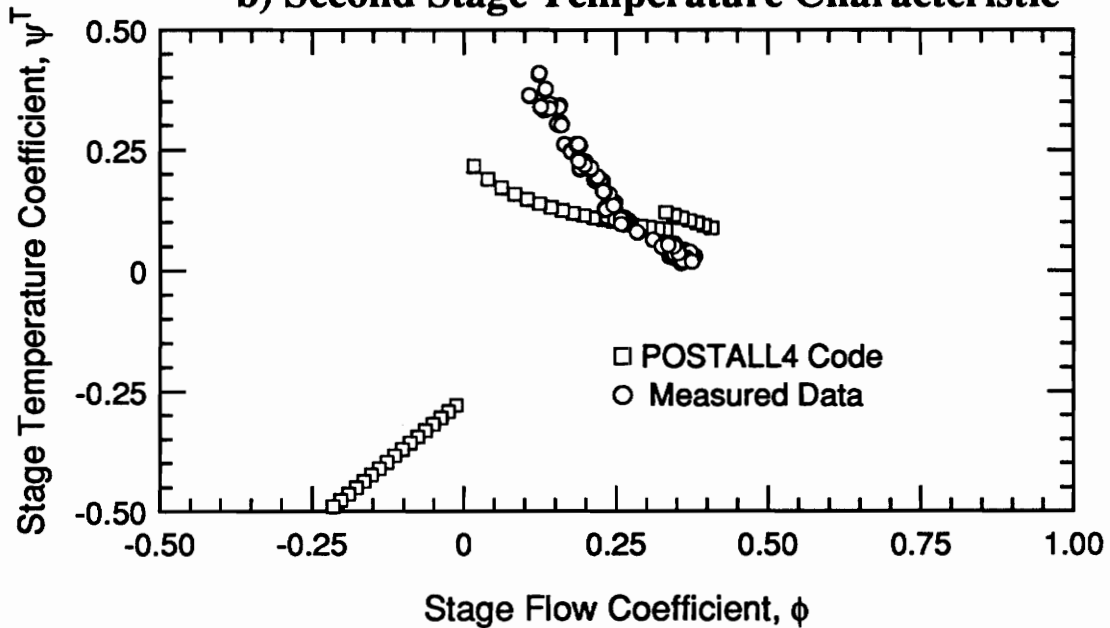
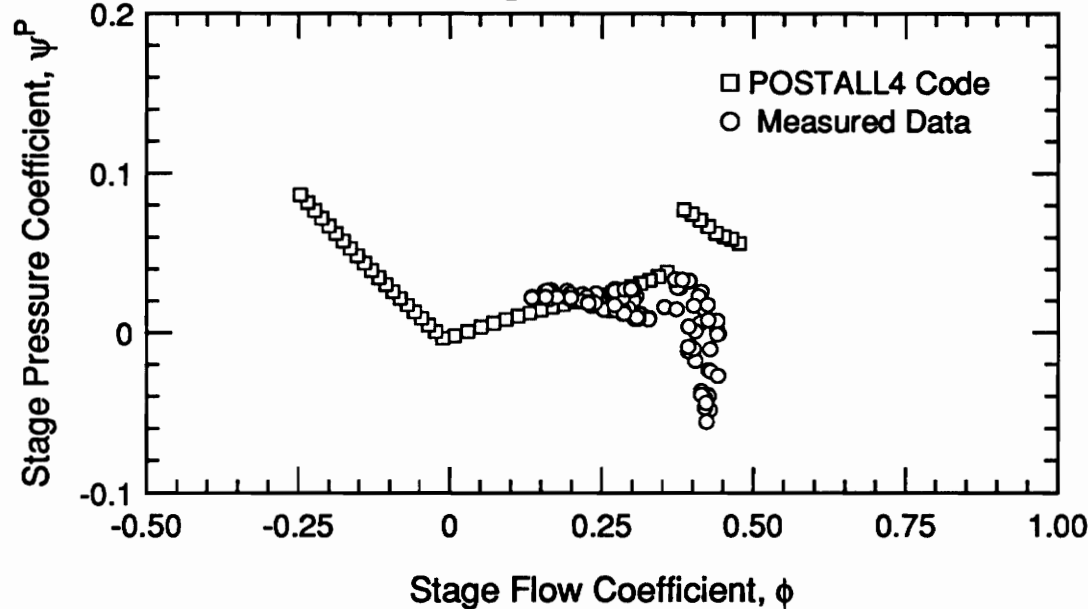


Figure 23. 10-Stage Compressor: a) Second Stage Pressure Characteristic; b) Second Stage Temperature Characteristic

10-Stage Test Compressor

a) Third Stage Pressure Characteristic



b) Third Stage Temperature Characteristic

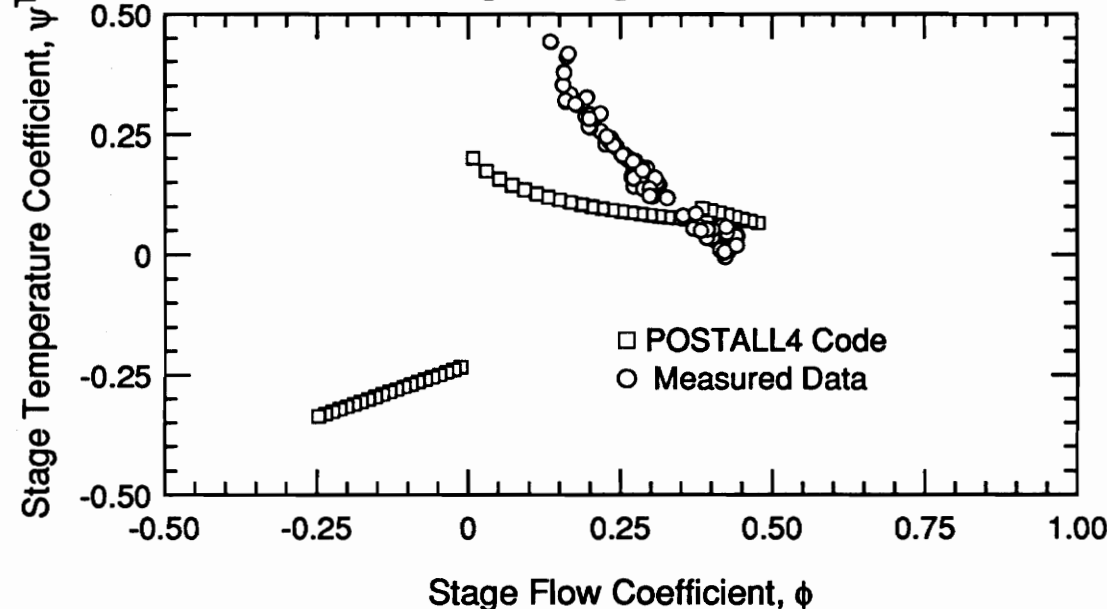
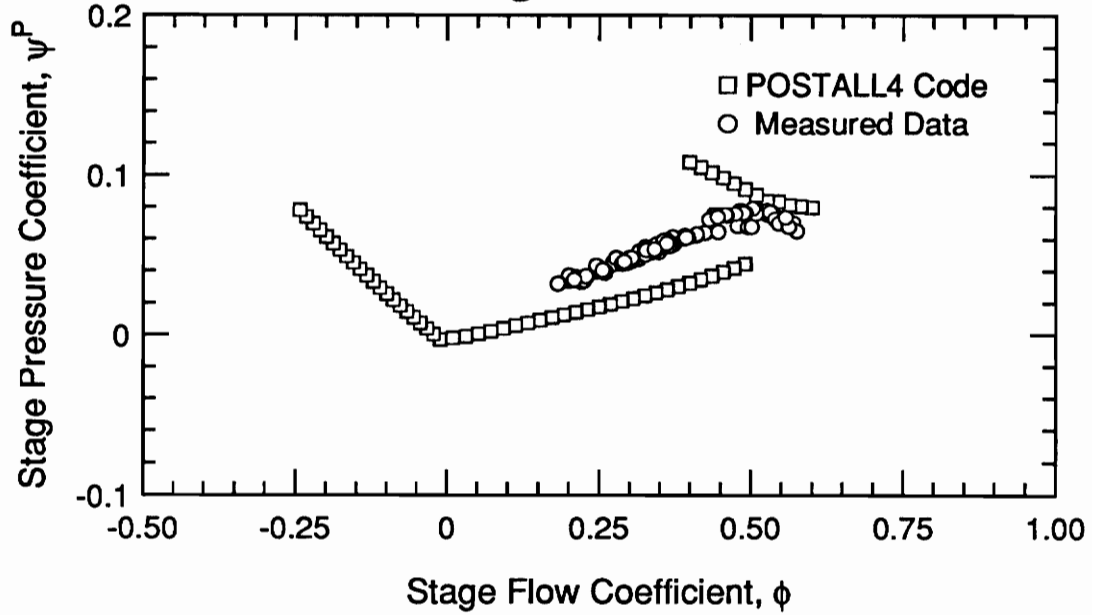


Figure 24. 10-Stage Compressor: a) Third Stage Pressure Characteristic; b) Third Stage Temperature Characteristic

10-Stage Test Compressor

a) Fourth Stage Pressure Characteristic



b) Fourth Stage Temperature Characteristic

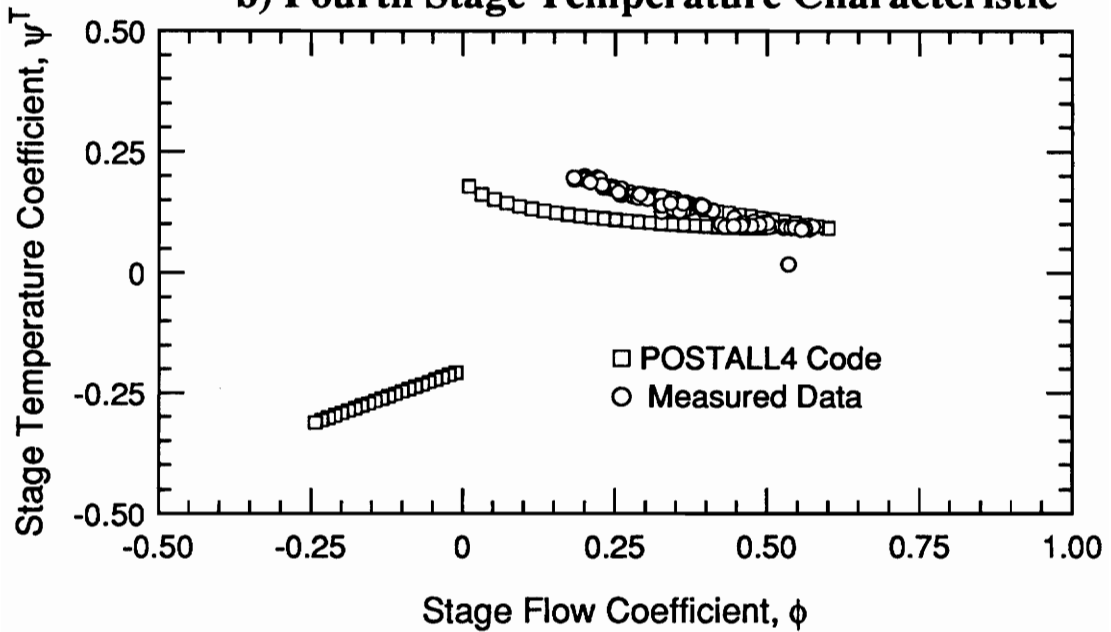
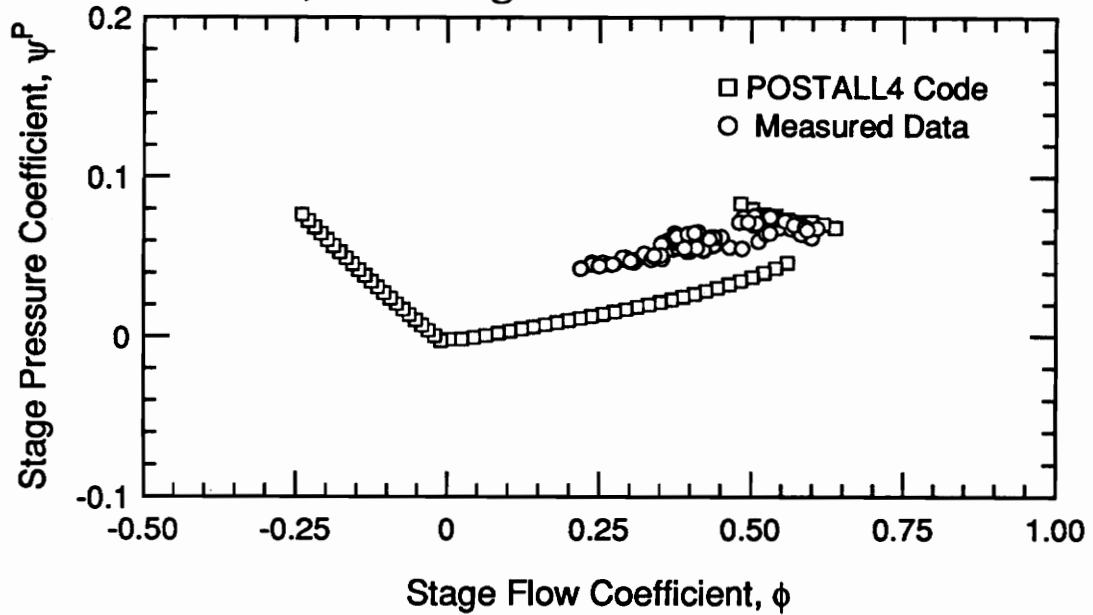


Figure 25. 10-Stage Compressor: a) Fourth Stage Pressure Characteristic; b) Fourth Stage Temperature Characteristic

10-Stage Test Compressor

a) Fifth Stage Pressure Characteristic



b) Fifth Stage Temperature Characteristic

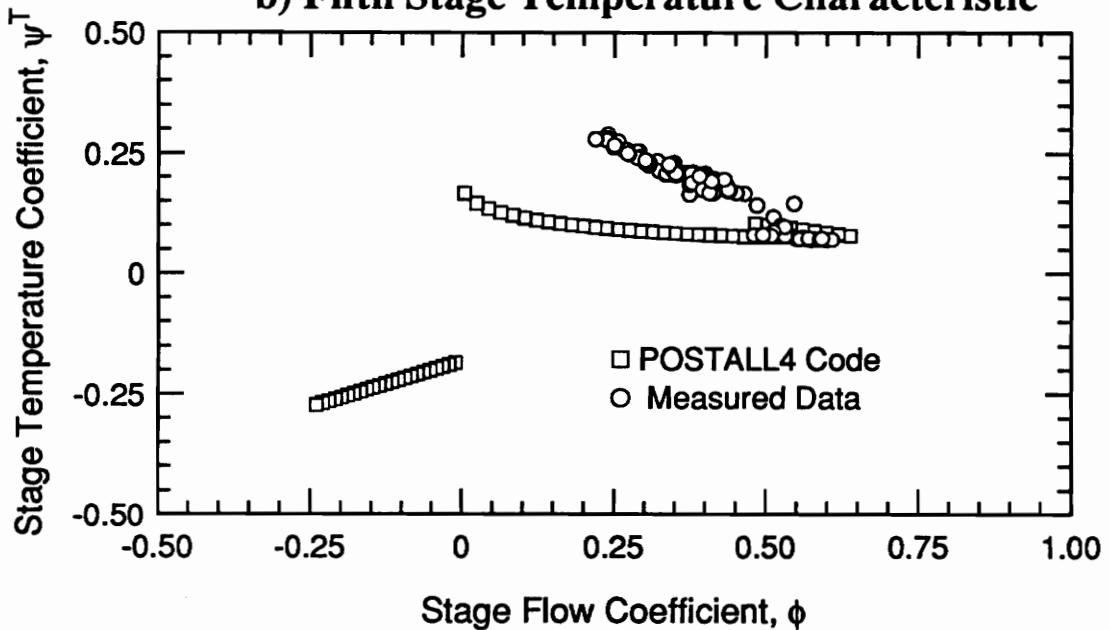
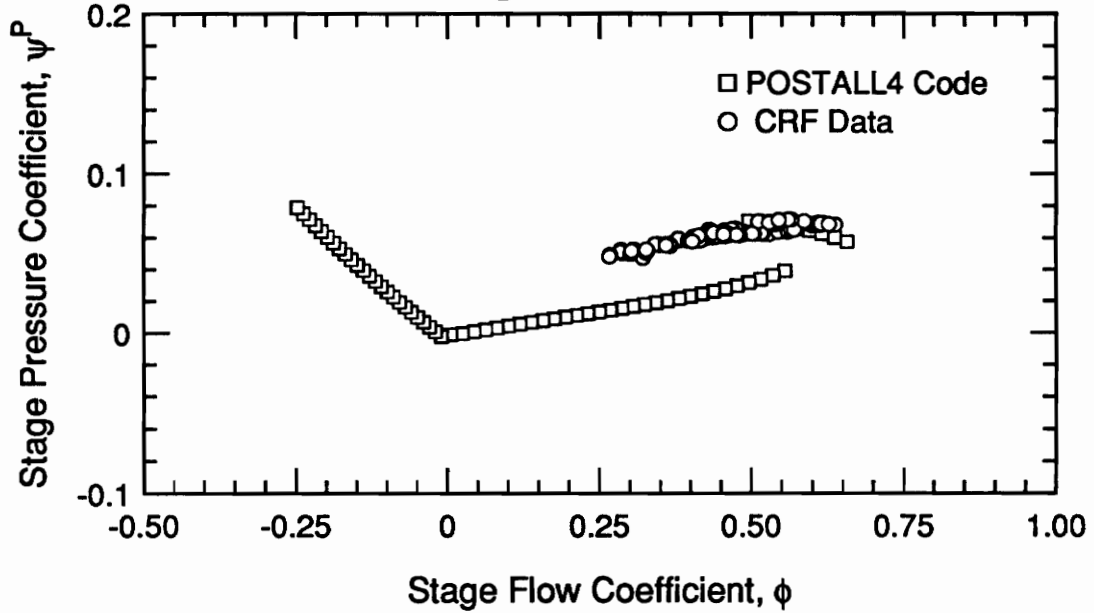


Figure 26. 10-Stage Compressor: a) Fifth Stage Pressure Characteristic; b) Fifth Stage Temperature Characteristic

10-Stage Test Compressor

a) Sixth Stage Pressure Characteristic



b) Sixth Stage Temperature Characteristic

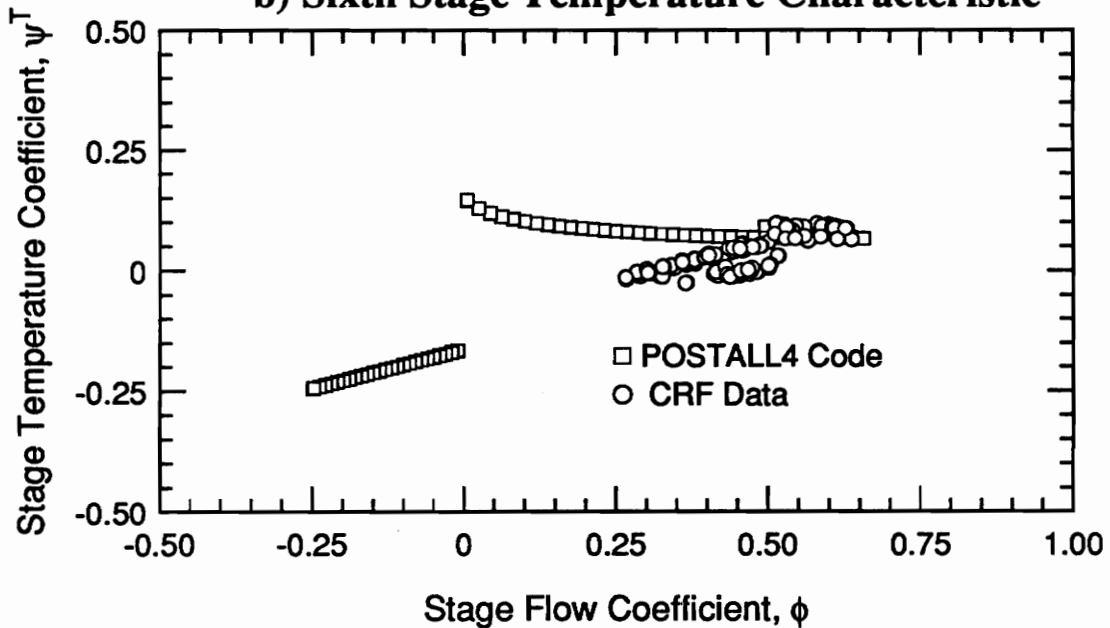
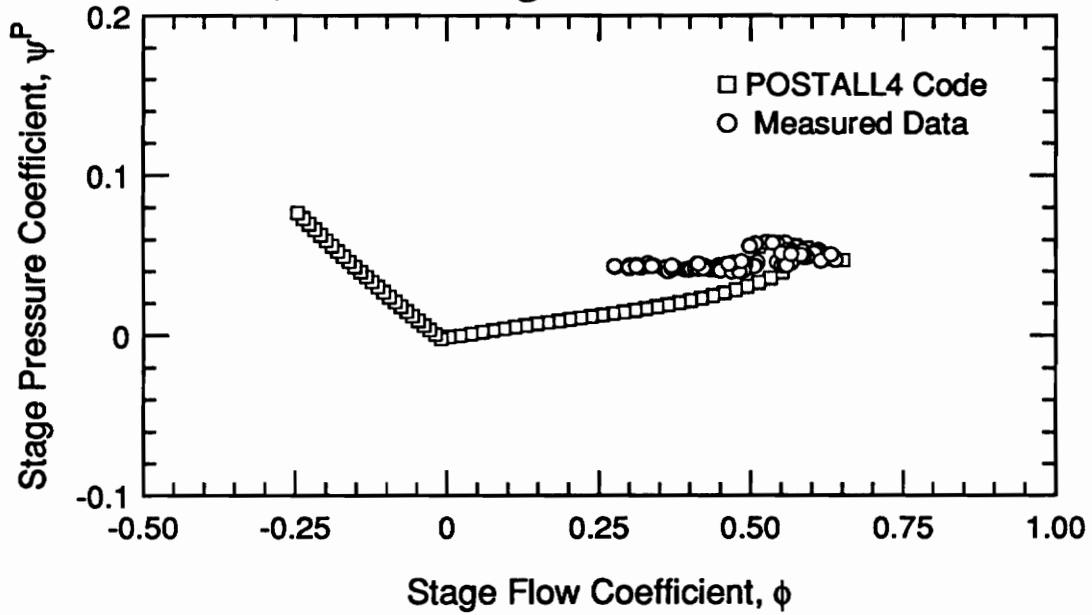


Figure 27. 10-Stage Compressor: a) Sixth Stage Pressure Characteristic; b) Sixth Stage Temperature Characteristic

10-Stage Test Compressor

a) Seventh Stage Pressure Characteristic



b) Seventh Stage Temperature Characteristic

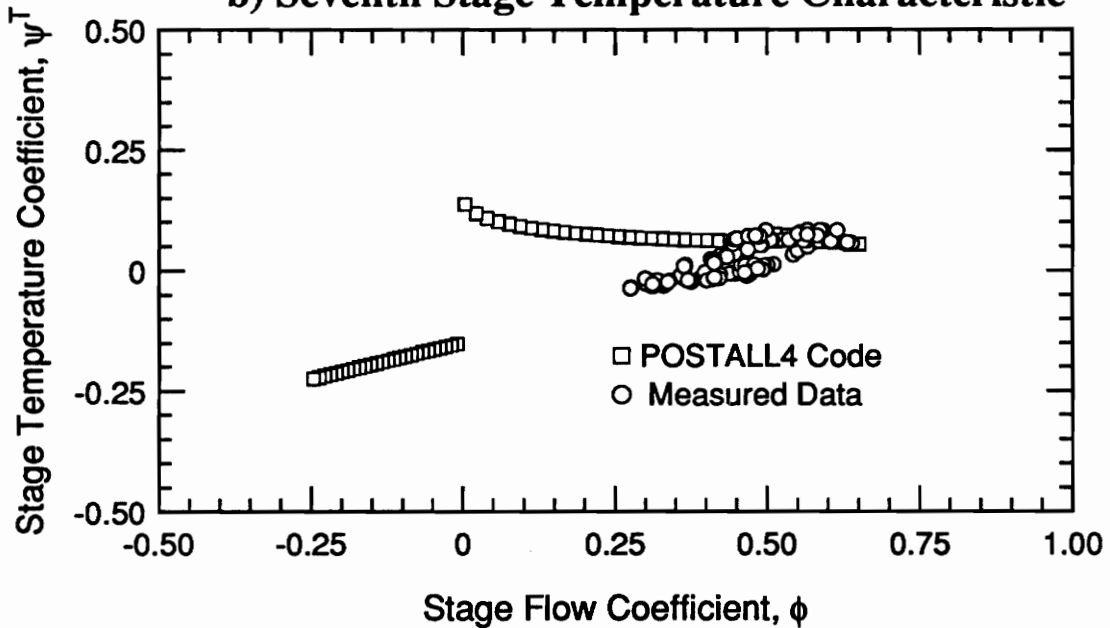
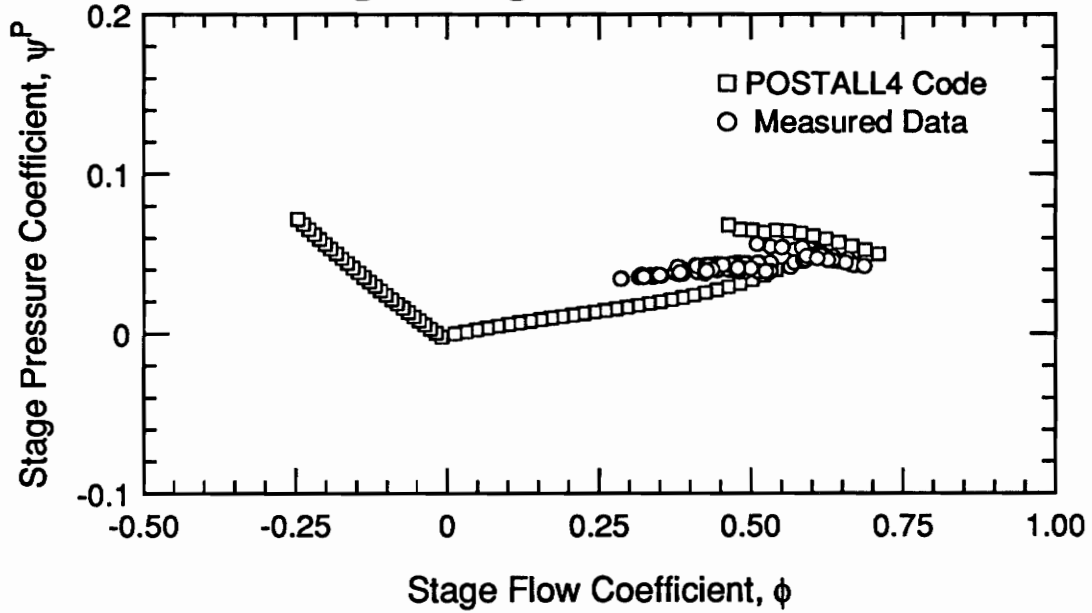


Figure 28. 10-Stage Compressor: a) Seventh Stage Pressure Characteristic; b) Seventh Stage Temperature Characteristic

10-Stage Test Compressor

a) Eighth Stage Pressure Characteristic



b) Eighth Stage Temperature Characteristic

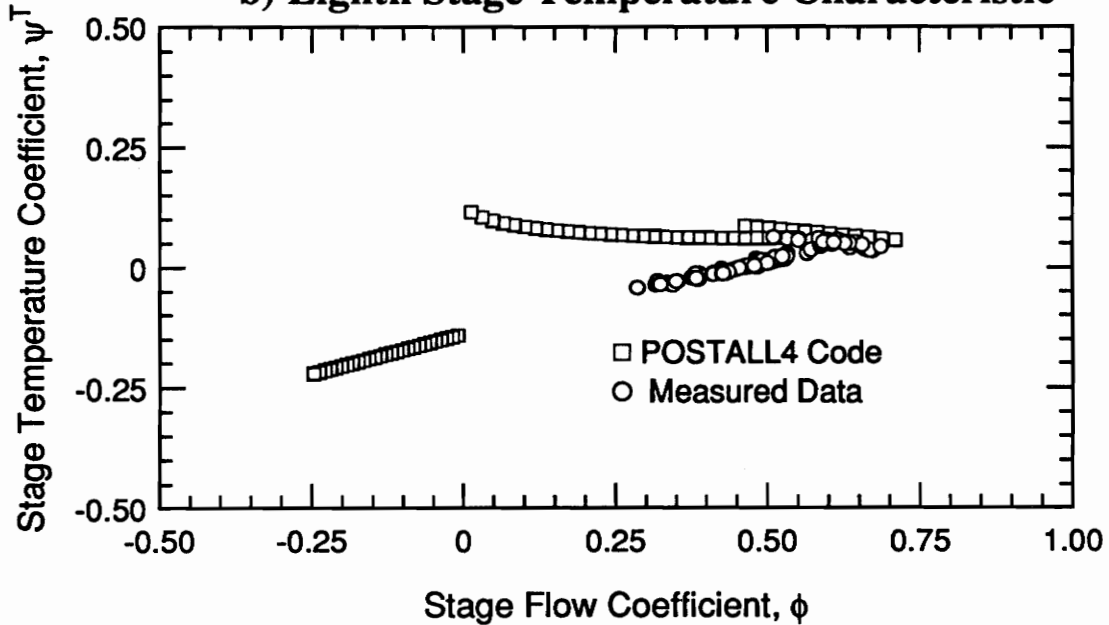
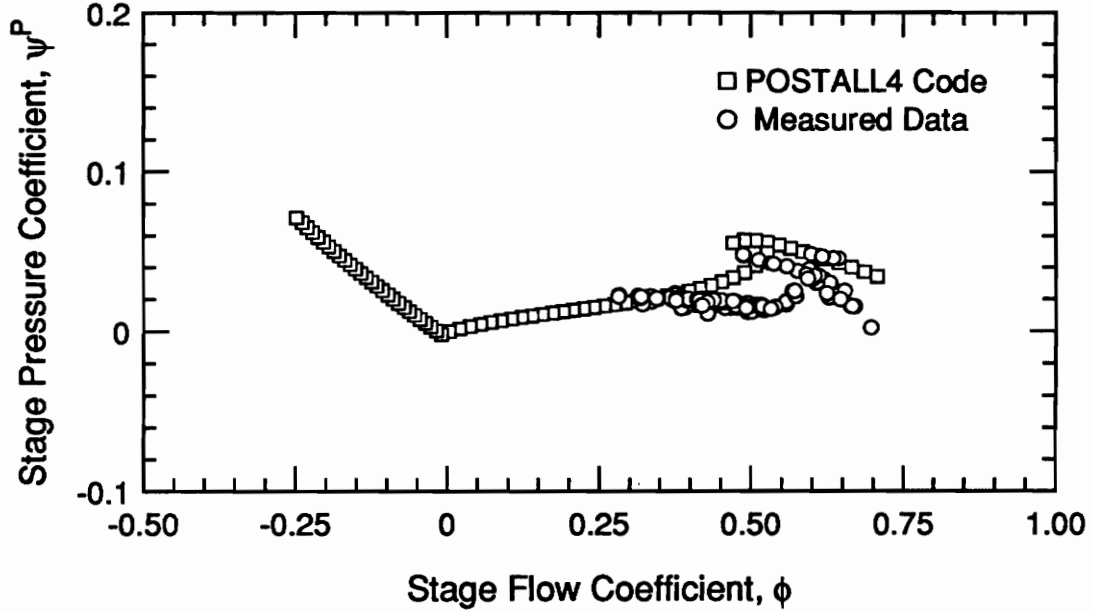


Figure 29. 10-Stage Compressor: a) Eighth Stage Pressure Characteristic; b) Eighth Stage Temperature Characteristic

10-Stage Test Compressor

a) Ninth Stage Pressure Characteristic



b) Ninth Stage Temperature Characteristic

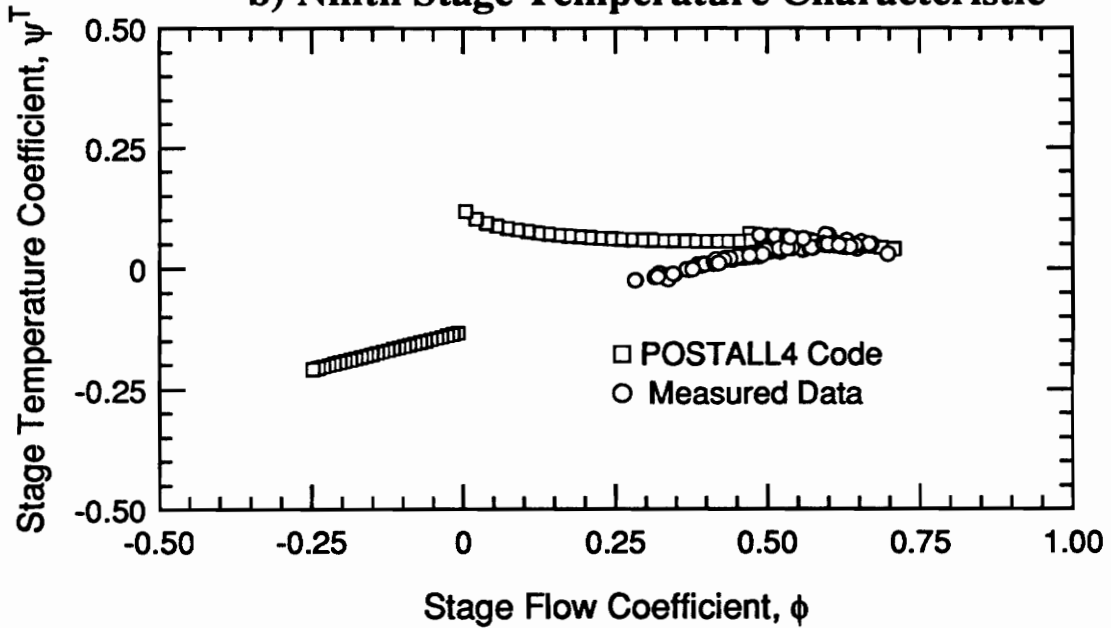
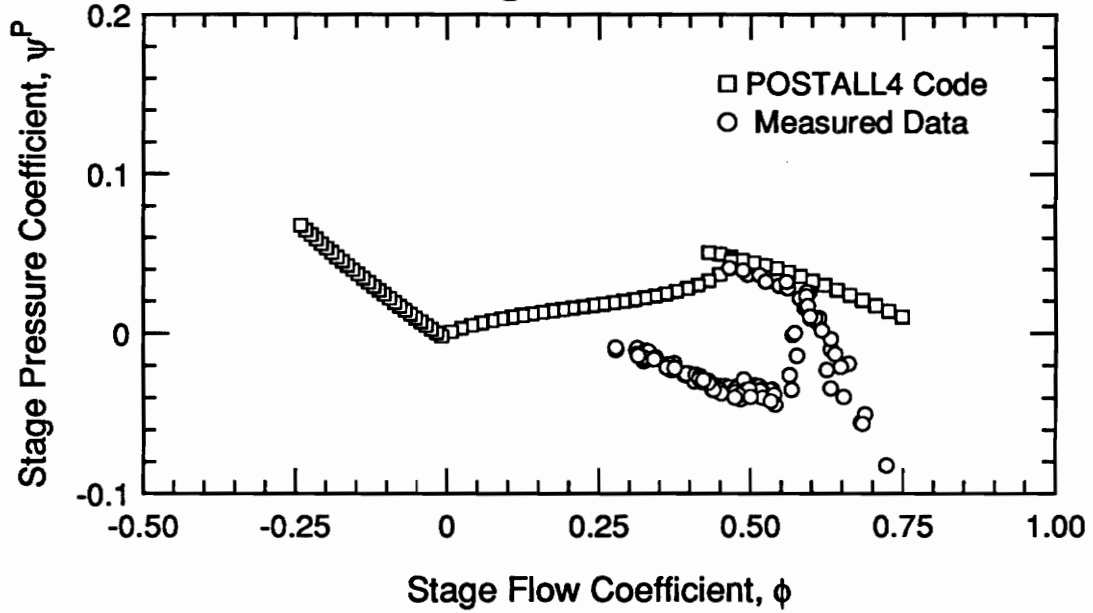


Figure 30. 10-Stage Compressor: a) Ninth Stage Pressure Characteristic; b) Ninth Stage Temperature Characteristic

10-Stage Test Compressor

a) Tenth Stage Pressure Characteristic



b) Tenth Stage Temperature Characteristic

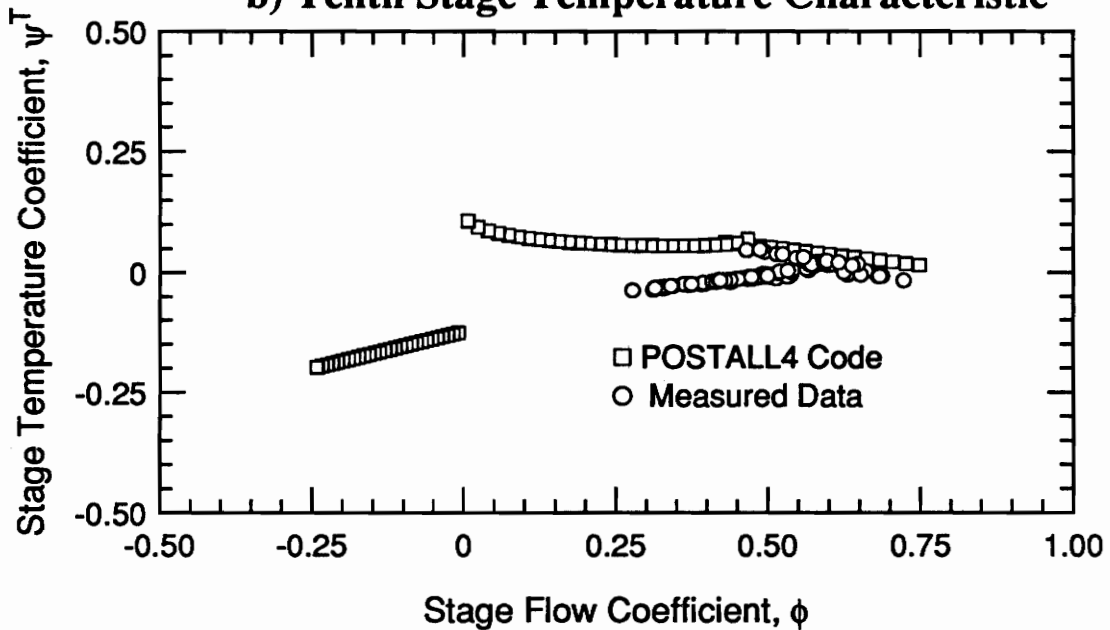


Figure 31. 10-Stage Compressor: a) Tenth Stage Pressure Characteristic; b) Tenth Stage Temperature Characteristic

6 PARAMETRIC INVESTIGATION OF DESIGN VARIABLES

In an effort to demonstrate the effects of changes in stage design variables on full range stage performance, a brief parametric investigation was conducted. The effects of small changes in rotor blade camber, solidity, and stagger were explored and the results are presented. To the best of the author's knowledge, this is the first parametric study of the effect of changes in design variables on full range stage performance.

6.1 The Effect of Camber on Full Range Performance

The effect of rotor blade camber on full range performance is presented in Figure 32 and the well-known trend of increased pressure rise with increased camber is obvious for the unstalled portion of the characteristic. The camber was increased by reducing the trailing edge blade angle while holding the leading edge blade angle and the stagger angle fixed; all other design variables were held fixed. Although there is a moderate difference in the pressure characteristics at the higher flow coefficients, it is interesting to note that the turning losses for the more highly cambered blade increase significantly just before stall, resulting in almost identical pressure rise at the stall point for all three stages.

The effect of increased camber is evident on the in-stall characteristics, but it is much less marked than in the unstalled regime. This is because the flow deviation angle increases dramatically when a blade row stalls and the more highly cambered blades are unable to turn the flow significantly more than the blades with less camber.

As discussed in Section 3.2, reversed flow is assumed to leave the blade at the leading edge angle, so the reversed flow performance was unaffected by the above changes in blade trailing edge angle.

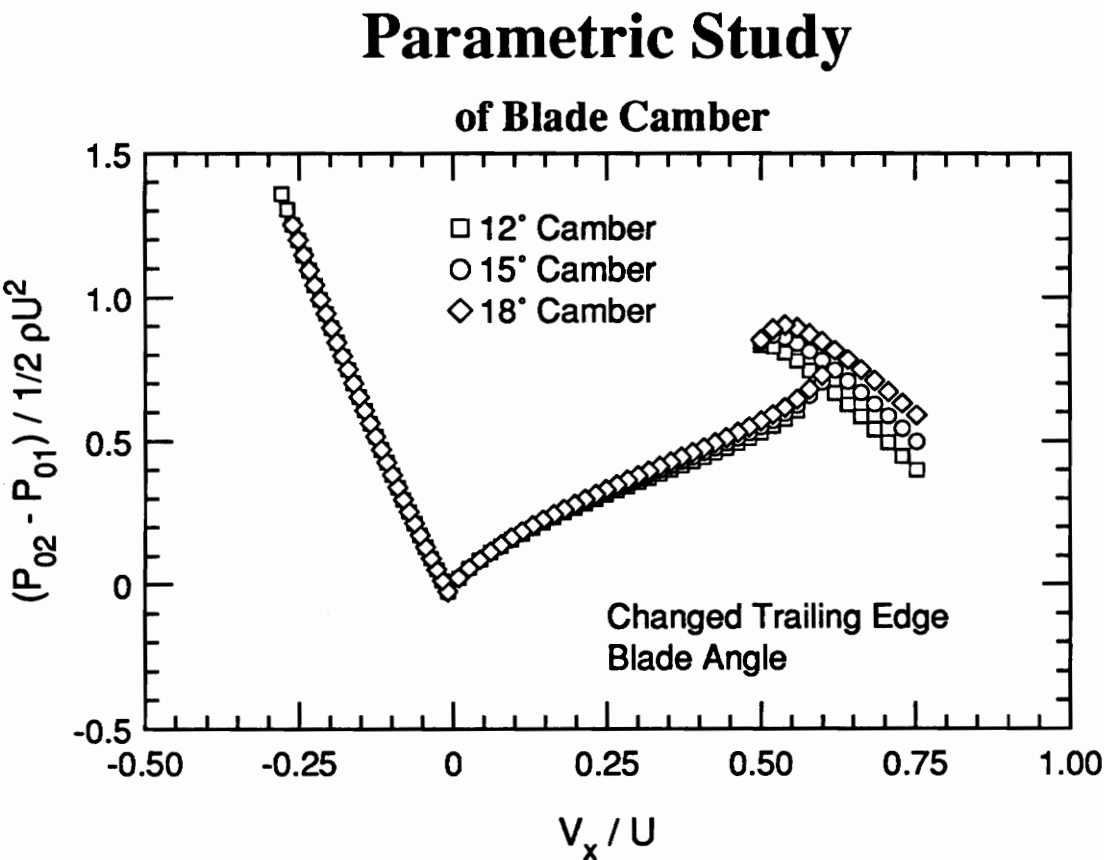


Figure 32. The Effect of Rotor Blade Camber on Full Range Stage Performance

6.2 The Effect of Rotor Solidity on Full Range Performance

To study the effects of rotor solidity on stage performance, the number of rotor blades was varied while all other variables were held constant; the resulting stage characteristics are shown in Figure 33. In the unstalled flow regime, there are two opposing trends which affect stage performance. A stage with higher solidity will have a

lower deviation angle than one with lower solidity, resulting in more turning of the flow, but the profile losses will be higher because there are more blades in the flow. At the higher flow coefficients, where the flow enters at a small angle of incidence, the losses are fairly low and the increased turning creates a higher pressure rise. At the lower unstalled flow rates, where the flow incidence is larger, the increased profile losses for the higher solidity stages dominate the turning and the pressure characteristic "turns over" just before stalling occurs.

Parametric Study of Blade Solidity

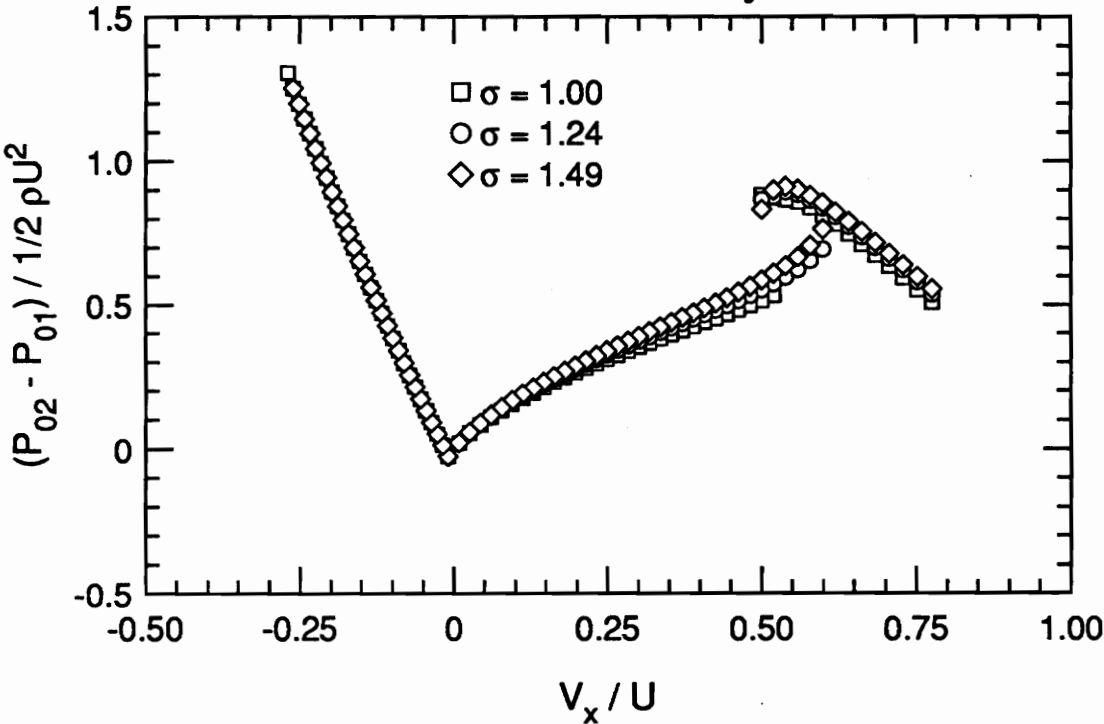


Figure 33. The Effect of Rotor Blade Solidity on Full Range Stage Performance

In the stalled regime, the deviation angle is large and the actual turning of the flow is small. In this region, the increased turning ability of the higher solidity stages is

the dominant factor. It is interesting to note, however, that there is a range of the stalled characteristic in which the POSTALL4 model predicts a *lower* profile loss for the higher solidity stages than for the lower solidity stages. This trend is consistent with the data reported by Ainslie [19].

As discussed in Section 3.2, reversed flow is assumed to leave the blade at the leading edge angle, and the losses are approximated as a function of mass flow only, so the reversed flow performance was unaffected by the above changes in solidity.

6.3 The Effect of Stagger on Full Range Performance

The effect of changing the blade stagger angle was investigated by changing both the rotor and stator blade leading, trailing, and stagger angles by the same amount simultaneously; all other design variables were unchanged. Although the intent of this investigation was to show the effect of changing rotor stagger only, the ensuing flow angles at the stator entrance would have resulted in stator operation far from design when the rotor was operating near design. For this reason, the stagger of both blades was varied.

The effect of changing blade stagger can be understood by considering the velocity triangles shown in Figure 34. For a given rotor incidence, the blade with a larger stagger angle (as measured from an axial reference) will have a larger relative flow angle, β_1 , and a smaller mass flow coefficient, V_x/U . Since the blades are the same, other than the stagger angle, the rotor turning will be nearly the same for both cases. If the change in absolute flow angle at the blade exit, α_2 , is not sufficient to stall the stator (which was also re-staggered), the difference in stator loss will be small and the stage pressure rise will be approximately the same for both cases. The overall result will be that the pressure characteristic in the forward flow regime will be shifted to the left on the mass flow axis.

For the three stagger angles considered in this study, the characteristics are essentially identical in the unstalled region, but shifted progressively left on the mass flow axis, as shown in Figure 35. It is interesting to note that the differences between the stalled characteristics diminishes as the flow coefficient is decreased. It is believed that this may be caused by the increased deviation in-stall producing nearly the same fully-mixed flow angle for a given mass flow coefficient, regardless of stagger, but this is not well understood at this time.

Although the leading edge blade angle was slightly different for each of the three stages, the reversed flow predictions are nearly coincident. This is consistent with the reversed flow characteristics of the first and second stages of the Gamache [8] compressor, which are also coincident in spite of their differing blade geometry.

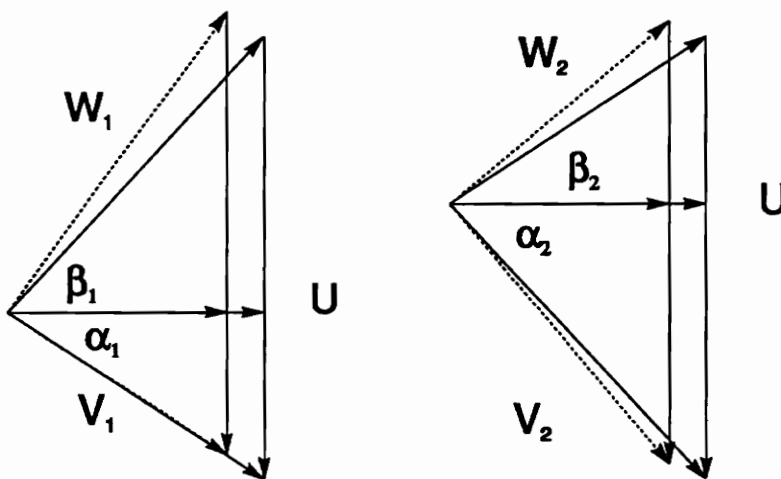


Figure 34. Velocity Triangles Showing Effect of Increased Stagger

Parametric Study of Blade Stagger

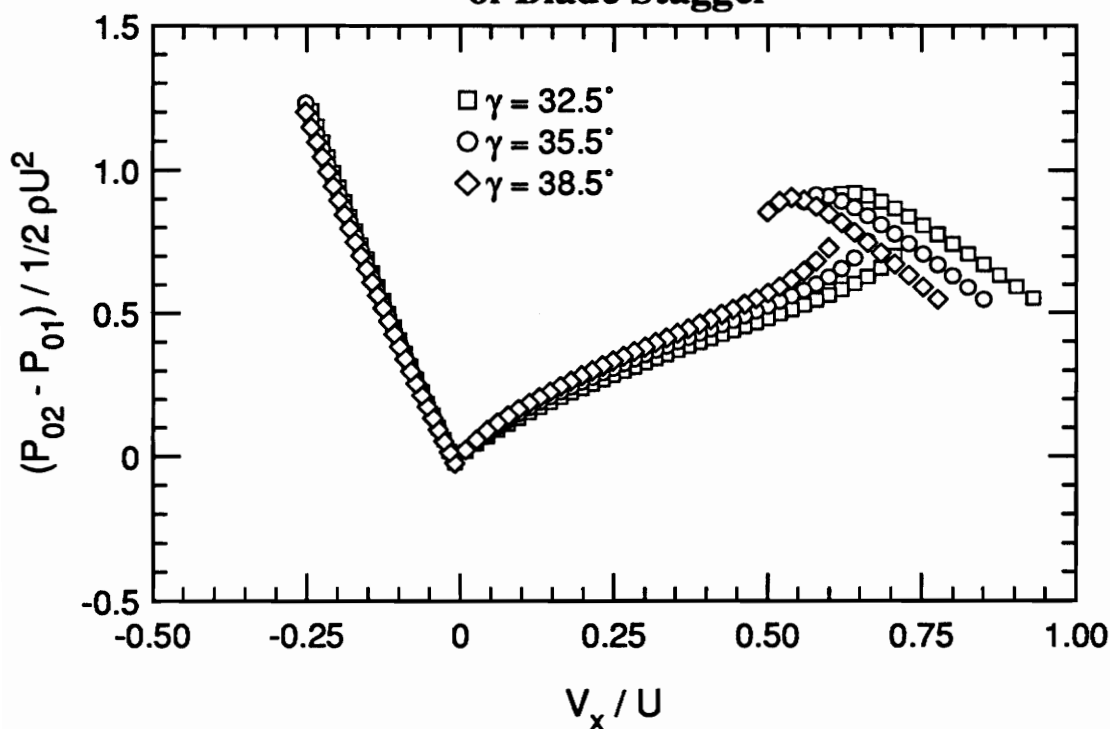


Figure 35. The Effect of Stagger on Full Range Stage Performance

7 CONCLUSIONS

A model for predicting the wide range characteristics, including in-stall and reversed flow, of axial flow compressor stages has been developed and a parametric study of the effect of changing camber, solidity, and stagger on steady state performance has been conducted. The unstalled characteristics show the well-known effects of these changes, but the effects are much less pronounced in the stalled flow regime. For moderate changes in these variables, the reversed flow characteristics are essentially unchanged.

The model was applied to a 3-stage low-speed compressor and very good agreement with the measured characteristics was shown. The prediction of the reversed flow characteristics was essentially identical to the measured performance.

The model was applied to a 10-stage high-speed compressor and mixed results were shown. There were effects of compressibility apparent in the forward stages which could not be captured by the current model. The predicted pressure characteristics showed very good agreement with the unstalled performance of the last five stages, although the tenth stage characteristics diverged at high mass flows. The in-stall prediction was positively sloped and similar for all stages, but the measured performance was dependent on the stage location. The reversed flow pressure characteristics are in good qualitative agreement with those of the low-speed compressor modeled, but no high-speed data exists in the open literature for this flow regime.

The unstalled temperature predictions for the first five stages showed the correct trends, but were larger than the measured performance. At low flow rates, the model under-predicted the temperature rise by a substantial amount; it is believed that this is the effect of significant viscous heating which is not captured by the model. The unstalled

temperature characteristics for the last five stages were in excellent agreement with the measured performance, but the in-stall performance indicated a significant amount of recirculating flow in the rotating stall cells which could not be predicted by the steady-state, two-dimensional code.

As mentioned above, the unstalled temperature predictions for the ninth and tenth stages were very close to the measured values, but the pressure characteristics did not show the same level of agreement. It is suggested that the stage losses, and hence the performance, are a function of the environment in which the stage is operated, as well as the stage itself.

The stage temperature characteristic is essentially linear in the unstalled operating region, but has a discontinuous change in slope and curvature at the inception of progressive stall. Because a stage can operate in-stall with a negatively sloped pressure characteristic, it is suggested that the temperature characteristic might be a better indicator of stall inception.

When a stage stalls, it upsets the flow field downstream to a sufficient extent that it can drive the next downstream stage into stall, even if the downstream stage was operating away from its stall point. For this reason it is suggested that there are certain points on the steady state stage characteristics which cannot be reached in a multi-stage environment. This is complimentary to the conclusion that a stage operated in a multi-stage environment could operate unstalled at flows significantly below the isolated clean-flow stall point, as reported by Longley and Hynes [28].

8 RECOMMENDATIONS

Preliminary application of this model has shown encouraging agreement, but further model validation is necessary. Subsequent application of this model is limited by the lack of full range data with which comparisons can be made. Compression system testing should be extended to include the in-stall and reversed flow regimes.

There are two areas in which further model development is necessary. The effects of compressibility appear to be significant in high-speed multi-stage compressors, even when operated at part speed. A proposed method for including compressibility effects is presented in Appendix A and should be developed. In high speed compressors operated at low mass flow, the effects of viscous heating appear to be significant and the model should be modified to include this effect.

The effects of changes in design variables on unstalled steady state performance are well known. As a result of the present investigation, a model for predicting the effects of these changes on full range performance is now available and an in-depth parametric study should be conducted. The steady state stage characteristics that result from this parametric investigation should be used as inputs to dynamic compression system models to examine the effects on unstalled transient response, stalling and recovery.

When a stage is operating unstalled, the temperature characteristic is essentially linear. When the stage stalls, the temperature characteristic shows a discontinuous change in slope and concavity which is far more evident than the change in slope of the pressure characteristic. In fact, it is possible for the pressure characteristic to have a negative slope while the stage is operating in-stall. It is suggested that the temperature characteristic may be a better indicator of stall inception than the pressure characteristic, but this concept should receive further study.

The current model is based on two-dimensional axisymmetric assumptions. Work to include two- and three-dimensional nonuniform effects, especially the non-axisymmetric blockage of rotating stall, should be pursued.

REFERENCES

1. Saravanamuttoo, H. I. H., and A. J. Fawke, "Simulation of Gas Turbine Dynamic Performance," ASME Paper 70-GT-23.
2. Seldner, K., J. R. Mihalow, and R. J. Blaha. "Generalized Simulation Technique for Turbojet System Analysis," NASA TN D-6610, February 1972.
3. Kimzey, W. F. "An Analysis of the Influence of Some External Disturbances on the Aerodynamic Stability of Turbine Engine Axial Flow Fans and Compressors," Arnold Engineering Development Center TR-77-80, August 1977.
4. Turner, R. C. and D. W. Sparkes. "Complete Characteristics For a Single-Stage Axial-Flow Fan," Thermodynamics and Fluid Mechanics Convention, Proceedings of the Institution of Mechanical Engineers, Cambridge, England, April 9-10, 1964.
5. Huppert, M. C. "Compressor Surge," Chapter XII of Aerodynamic Design of Axial Flow Compressors, NASA SP-36, 1965.
6. Greitzer, E. M. "Surge and Rotating Stall in Axial Flow Compressors, Part I: Theoretical Compression System Model," Journal of Engineering for Power, April 1976, pp. 190-198.
7. Greitzer, E. M. "Surge and Rotating Stall in Axial Flow Compressors, Part II: Experimental Results and Comparison With Theory," Journal of Engineering for Power, April 1976, pp. 199-217.
8. Gamache, R. N. "Axial Compressor Reversed Flow Performance," Ph.D. Dissertation, M.I.T., May 1985.
9. Davis, M. W. "A Stage-by-Stage Post-Stall Compression System Modeling Technique: Methodology, Validation, and Application," Ph.D. Dissertation, V.P.I.&S.U., December 1986.
10. Browell, R. W., L. D. Reynolds, and W. P. Core. "COCODEC: Combined Compressor Design and Evaluation Code," Union Carbide Corporation, Nuclear Division, CTC-INF-1039, May 1972.

11. Boyer, K. M., and W. F. O'Brien. "Model Predictions for Improved Recovery of a Multistage Axial-Flow Compressor," AIAA Paper No. 89-2687, 1989.
12. Dowler, C. A., K. M. Boyer, and N. Poti. "Model Predictions of Fan Response To Inlet Temperature Transients and Spatial Temperature Distortion," AIAA Paper No. 89-2686, 1989.
13. Copenhaver, W. W. "Stage Effects on Stalling and Recovery of a High-Speed 10-Stage Axial Flow Compressor," Ph.D. Dissertation, Iowa State University, 1988.
14. Hill, P. G., and C. R. Peterson, Mechanics and Thermodynamics of Propulsion, Addison Wesley, 1965.
15. Lieblein, S. "Loss and Stall Analysis of Compressor Cascades," Transactions of the ASME, Journal of Basic Engineering, September 1959, pp. 387-400.
16. Horlock, J. H. Axial Flow Compressors, Robert E. Krieger Publishing Company, 1973.
17. Robins, W. H., and J. F. Dugan. "Prediction of Off-Design Performance of Multistage Axial Flow Compressors," Chapter X of Aerodynamic Design of Axial Flow Compressors, NASA SP-36, 1965.
18. Yocum, A. M. II. "An Experimental and Numerical Investigation of the Performance of Compressor Cascades With Stalled Flow," Ph.D. Dissertation, V.P.I.&S.U., May 1988.
19. Ainslie, W. E. "The Effect of Solidity on the Pre- and Post-Stall Flow in a Linear Compressor Cascade," M.S. Thesis, V.P.I.&S.U., August 1988.
20. Moses, H. L., and S. B. Thomason. "An Approximation for Fully Stalled Cascades," Journal of Propulsion, March-April 1986, pp. 188-189.
21. Carneal, J. P. "Experimental Investigation of Reversed Flow in a Compressor Cascade," M.S. Thesis, V.P.I.&S.U., June 1990.
22. Koff, S. G., and E. M. Greitzer. "Axisymmetrically Stalled Flow Performance for Multistage Axial Compressors," Journal of Turbomachinery, October 1986, pp. 216-223.
23. O'Brien, W. F. "Compressor Post Stall Model," Final Report for Sverdrup Technology, Inc., September 1987.

24. Lieblein, S. "Experimental Flow in Two-Dimensional Cascades," Chapter VI of Aerodynamic Design of Axial Flow Compressors," NASA SP-36, 1965.
25. Koch, C. C., and L. H. Smith. "Loss Sources and Magnitudes in Axial-Flow Compressors," *Journal of Engineering for Power*, July 1976, pp. 411-424.
26. Dixon, S. L. Fluid Mechanics. Thermodynamics of Turbomachinery, Pergammon Press, 1975.
27. Bloch, G. S. "Compressor Stage Characteristics Prediction," V.P.I.&S.U. Center for Turbomachinery and Propulsion Research Report No. 901201, December 1990.
28. Longley, J. P., and T. P. Hynes. "Stability of Flow Through Multistage Axial Compressors," *Journal of Turbomachinery*, January 1990, pp. 126-132.
29. Cousins, W. T. private communication, April 1991.
30. Graham, R. W., and E. C. Guentert. "Compressor Stall and Blade Vibration," Chapter XI of Aerodynamic Design of Axial Flow Compressors," NASA SP-36, 1965.

APPENDIX A

AN APPROACH FOR A COMPRESSIBLE FLOW STAGE PERFORMANCE MODEL

During the application of the POSTALL4 model to a 10-stage, high speed compressor, the effects of compressibility were encountered. Because it appears that a stage performance model which cannot account for density variation will probably not be able to accurately predict the behavior of high speed compressors, it is suggested that a compressible model be developed. The following is a brief description of a possible method for including the effects of compressibility in a stage characteristics prediction model.

Because the notation can be somewhat confusing, the following description of subscript notation is given. The subscript tr will be used to denote total properties defined the relative reference frame. The subscripts 1 and 2 will be used to refer to the blade row inlet and outlet, respectively. Properties with a subscript of 0 are total properties to be used in a general equation which holds regardless of reference frame and the appropriate values should be substituted when performing the calculations. Properties with no subscript other than a 1 or 2 are static properties.

A typical compressor stage and the flow angles for forward flow is shown in Figure 36. The flow is assumed to enter the IGV axially with atmospheric total pressure and temperature. The axial Mach number is assumed and the method that follows is used to calculate the performance for one mass flow coefficient. To obtain the entire characteristic, the calculations are repeated for a range of inlet Mach numbers.

With the knowledge of the inlet Mach number, a mass flow parameter can be calculated as follows.

$$\frac{\dot{m}\sqrt{T_0}}{P_0 A} = M \sqrt{\frac{\gamma}{R} \left(\frac{1}{1 + \frac{\gamma-1}{2} M^2} \right)^{\frac{\gamma+1}{2(\gamma-1)}}} \quad (23)$$

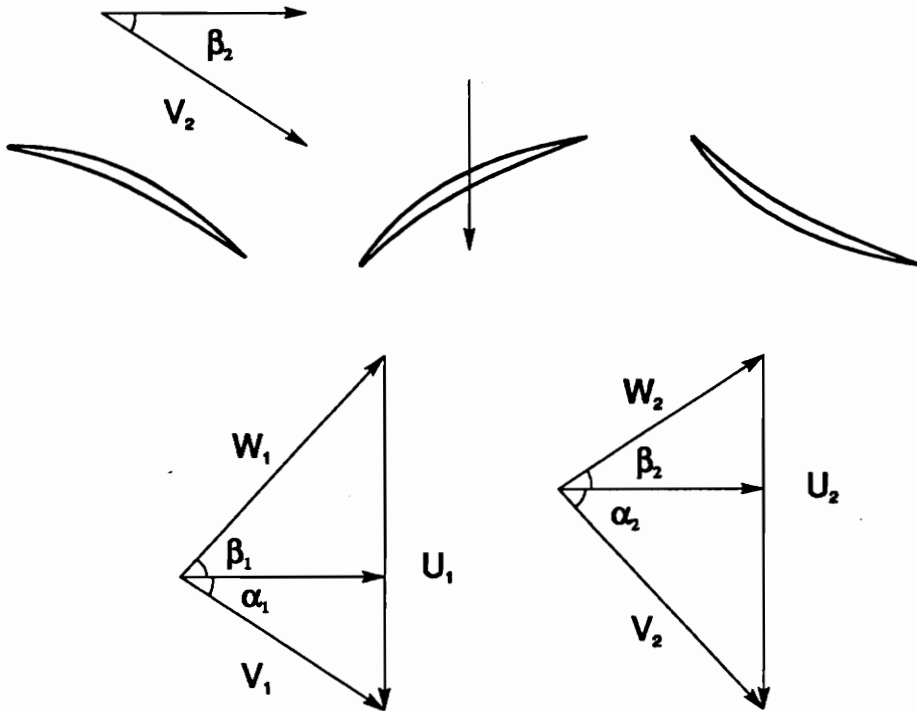


Figure 36. A Typical Compressor Stage With Velocity Triangles for Forward Flow Operation

With the inlet total temperature known (and the assumption of axial flow at the inlet), the inlet axial velocity can be calculated.

$$\frac{W}{\sqrt{c_p T_0}} = M \sqrt{\frac{\gamma - 1}{1 + \frac{\gamma - 1}{2} M^2}} \quad (24)$$

With a knowledge of the loss coefficient and flow deviation angle, the total pressure ratio and the area ratio can be calculated.

$$\frac{P_{r2}}{P_{r1}} = 1 - \overline{\omega} \left(1 - \frac{P_1}{P_{r1}} \right) \quad (25)$$

$$\frac{A_{r2}}{A_{r1}} = \frac{A_2 \cos \beta_2}{A_1 \cos \beta_1} \quad (26)$$

As stated above, the relative flow angle at the IGV inlet, β_1 , is assumed to be zero. Because a stationary blade cannot do work on the fluid, the total temperature does not change and the mass flow parameter at the IGV exit can be calculated.

$$\left(\frac{\dot{m} \sqrt{T_0}}{P_0 A} \right)_2 = \left(\frac{\dot{m} \sqrt{T_0}}{P_0 A} \right)_1 \left(\frac{P_{r1}}{P_{r2}} \right) \left(\frac{A_{r1}}{A_{r2}} \right) \quad (27)$$

The relative Mach number at the IGV exit can then be calculated from Equation (23) and the velocity at the IGV exit from Equation (24). For a stationary blade row, the relative reference frame is the same as the absolute frame the total pressure in the absolute frame is known from Equations (25). The static pressure and temperature at the IGV exit are calculated from the Mach number.

$$\frac{P_0}{P} = \left(1 + \frac{\gamma-1}{2} M^2\right)^{\frac{\gamma}{\gamma-1}} \quad (28)$$

$$\frac{T_0}{T} = 1 + \frac{\gamma-1}{2} M^2 \quad (29)$$

The relative velocity at the IGV exit is calculated from Equation (24) and the axial velocity and axial Mach number are calculated from trigonometry.

$$V_{x2} = W_2 \cos \beta_2 \quad (30)$$

$$M_{2x} = M_{2rel} \cos \beta_2 \quad (31)$$

The exit properties from the IGV are used as inlet conditions for the rotor. The relative flow angle and relative Mach number at the rotor inlet are calculated from trigonometry.

$$\beta_1 = \tan^{-1} \left(\frac{U_1}{V_{x1}} - \tan \alpha_1 \right) \quad (32)$$

$$M_{1rel} = \frac{M_{1x}}{\cos \beta_1} \quad (33)$$

The mass flow parameter in the relative frame at the rotor inlet is then calculated from Equation (23). The relative total pressure ratio is calculated from Equation (25) and the relative area ratio from Equation (26). With the assumption of constant rothalpy for the rotor, the relative temperature ratio can be calculated.

$$\frac{T_{r2}}{T_{r1}} = 1 + \frac{U_2^2 - U_1^2}{2c_p} \quad (34)$$

The mass flow parameter at the rotor exit can then be calculated.

$$\left(\frac{\dot{m}\sqrt{T_0}}{P_0 A} \right)_2 = \left(\frac{\dot{m}\sqrt{T_0}}{P_0 A} \right)_1 \left(\sqrt{\frac{T_{r2}}{T_{r1}}} \right) \left(\frac{P_{r1}}{P_{r2}} \right) \left(\frac{A_{r1}}{A_{r2}} \right) \quad (35)$$

The relative Mach number at the rotor exit is then calculated from Equation (23), and the static pressure and temperature from Equations (28) and (29), respectively. The relative velocity at the rotor exit is calculated from Equation (24), and the axial velocity from Equation (30). The absolute flow angle and absolute Mach number are calculated from trigonometry.

$$\alpha_2 = \tan^{-1} \left(\frac{U_2}{V_{x2}} - \tan \beta_2 \right) \quad (36)$$

$$M_{2abs} = \frac{M_{2rel}}{\cos \alpha_2} \quad (37)$$

The conditions at the rotor exit are then used as inlet properties for the stator row and the process is repeated.

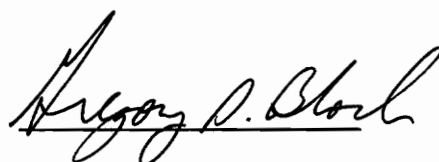
The method outlined above can be used to calculate the performance of an arbitrary number of blade rows and can be used to predict overall compression system performance, in addition to individual stage performance. The ability to examine a number of output coefficients, based on any combination of total or static properties, would also be available.

Some of the expected difficulties to be encountered with this model involve the propagation of information downstream. Any errors made in estimating the deviation angles and loss coefficients will propagate downstream and color the performance of the downstream stages. Also, when a blade row stalls, the downstream effects as they are currently calculated may result in discontinuities in the characteristic prediction.

VITA

The author, Gregory S. Bloch, was born in Quonset Point, Rhode Island on December 17, 1963. As the son of a U. S. Navy pilot, he traveled around the country during his childhood. The author entered Virginia Polytechnic Institute in the Fall of 1981 and squeezed a four year program into eight short years, receiving his B. S. in Mechanical Engineering in May 1989.

Mr. Bloch entered the Graduate School at V. P. I. in July 1989 and received his M. S. in Mechanical Engineering in August 1991. After completion of the M. S. program, he is going to work at the Propulsion Lab at Wright Patterson Air Force Base in Dayton, Ohio. After one year of training, the Air Force is sending him back to school to obtain his Ph. D.

A handwritten signature in black ink, reading "Gregory S. Bloch". The signature is written in a cursive style with a horizontal line underneath the name.

Gregory S. Bloch